24

Engineered Cementitious Composite (ECC): Material, Structural, and Durability Performance

Victor C. Li, Ph.D., FASCE, FASME, FWIF*

24.1 Historical Development

The development of fiber-reinforced concrete material has undergone a number of phases. In the 1960s, research by Romualdi and coworkers (Romualdi and Batson, 1963; Romualdi and Mandel, 1964) demonstrated the effectiveness of short steel fibers in reducing the brittleness of concrete. This development has continued with expansion to a variety of other fibers, such as glass, carbon, synthetics, natural fibers, and, in recent years, hybrids that combine either different fiber types or fiber lengths. The continuously enhanced knowledge of fiber-reinforcement effectiveness has resulted in structural design recommendations by RILEM TC 162-TDF (Vandewalle et al., 2003). This document focuses on fiber-reinforced

* E. Benjamin Wylie Collegiate Chair Professor, Department of Civil and Environmental Engineering, University of Michigan, Ann Arbor; expert on high-performance fiber-reinforced cementitious composites, inventor of engineered cementitious composites.

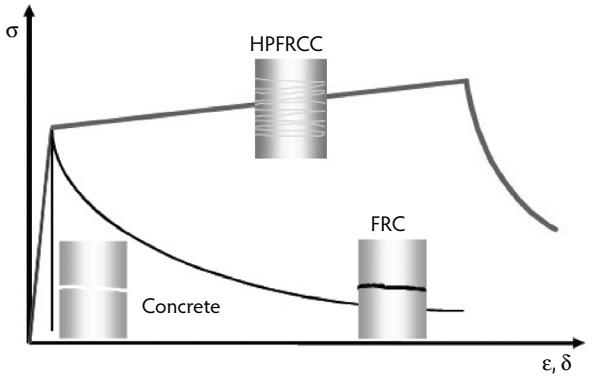

FIGURE 24.1 Uniaxial tensile stress–deformation relation of concrete, FRC, and HPFRCC. For FRC, deformation after a crack is formed is associated with crack opening δ. Tensile load capacity drops as a single crack enlarges during tension softening. For HPFRCC, deformation during the elastic and strain-hardening stages is properly described as straining. Tensile load capacity continues to rise during multiple microcracking and continued increase in strain. The strain capacity of HPFRCC is defined as the strain value at which peak tensile load is reached.

concrete (FRC) that possesses a tension-softening, quasi-brittle response (Figure 24.1). Apart from the gradual expanded use of the tension-softening branch of FRC in structural property enhancements, fibers in small quantities have been successfully used in controlling restrained drying shrinkage cracks. The subject of FRC is treated in detail in Chapter 22 of this book.

Beginning as early as the 1980s, interest in creating a fiber-reinforced concrete material with tensile ductility has been gaining ground. Within FRC, the toughness of the material is increased but no change in ductility is attained. Ductility is a measure of tensile deformation (strain) capacity typically associated with ductile steel, for example, but not with concrete material. Attempts to achieve tensile ductility in concrete material are exemplified by the early efforts of Aveston et al. (1971) and later Krenchel and Stang (1989), who demonstrated that, with continuous aligned fibers, high tensile ductility hundreds of times that of normal concrete can be attained. The modern-day version of continuous fiber reinforcement is represented by textile-reinforced concrete materials that may be prestressed (Curbach and Jesse, 1999; Reinhardt et al., 2003). Research on pultruded continuous fiber-reinforced concrete was pioneered by Mobasher et al. (2006). In parallel, research into the use of discontinuous fibers at high dosage (4 to 20%), such as in cement laminates (Allen, 1971) and in slurry-infiltrated fiber concrete (SIFCON) (Lankard, 1986; Naaman, 1992), has resulted in concrete composite materials that attain higher tensile strength than normal concrete and are not as brittle, but which have much less ductility than their continuous-fiber and textile-reinforced counterparts.

These materials may be considered a class of materials separate from FRC in that different degrees of tensile ductility are achieved, often accompanied by a strain-hardening response distinct from the tension-softening response of FRC. Naaman and Reinhardt (2003) classified such material as *high-performance fiber-reinforced cementitious composites* (HPFRCC) (Figure 24.1). It should be noted that most members of this class of material have a matrix that does not contain coarse aggregates and should therefore be regarded as fiber-reinforced cement pastes or mortars; however, in keeping with the broadened meaning used in the literature, we shall use the term *concrete material* in this chapter to include concrete, mortar, and cement paste.

Figure 24.1 illustrates the differences between the tensile response of normal concrete, FRC, and HPFRCC, such as obtained from a uniaxial tension test. This figure emphasizes the transition from brittle concrete to quasi-brittle FRC (tension softening) to ductile HPFRCC (strain hardening). Specifically, during tension softening, deformation is localized onto a single fracture plane, most appropriately described in terms of crack opening. During strain hardening, deformation is composed of the opening of multiple subparallel fine cracks and elastic stretching of the material between these cracks. Over a

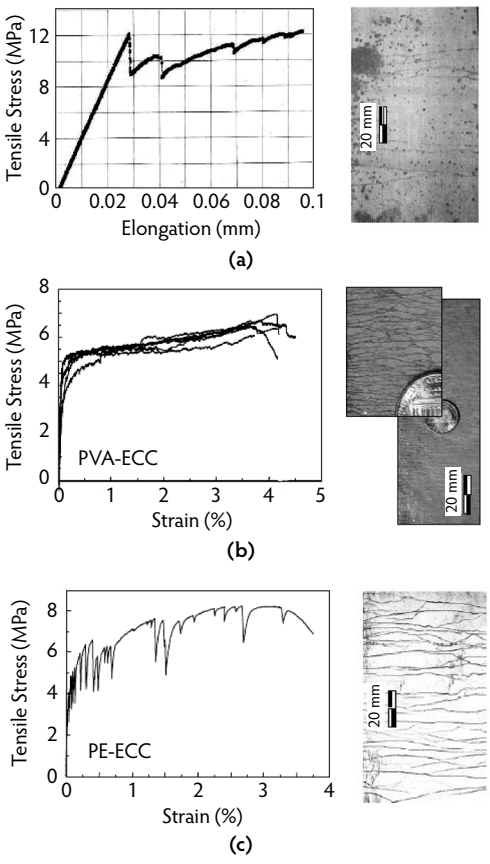

FIGURE 24.2 Two classes of HPFRCCs: (a) Tensile stress-elongation relationship for high-strength Ductal® based on prism specimen 70 × 70 × 160 mm with 150-mm gauge length. (Adapted from Chanvillard, G. and Rigaud, S., in *Proceedings of High-Performance Fiber-Reinforced Cement Composites (HPFRCC 4)*, Naaman, A.E. and Reinhardt, H.W., Eds., RILEM, Paris, 2003, pp. 21–34.) (b, c) Tensile stress–strain relationship for ductile ECC, based on coupon specimen 76 × 13 × 305 mm with 180-mm gauge length. (Adapted from Fischer, G. et al., in *Seventh International Symposium on Brittle Matrix Composites*, October 13–15, Warsaw, Poland, 2003, pp. 29–36; Li, V.C. and Wang, S., *ACI Mater. J.*, 99(1), 11–21, 2002.)

length scale that includes many such cracks, the deformation may be considered tensile strain smeared over a representative volume of material. As will be seen in the following sections, these distinctions between FRC and HPFRCC have significant ramifications in terms of load capacity and structural durability.

Whereas the HPFRCC materials mentioned above embody the highly desired tensile properties lacking in normal concrete or in FRC, until recently they have mostly been limited to academic research laboratories or specialized applications. This is due to additional demands in industrial projects, particularly in on-site construction, such as economical feasibility and constructability. These two demands are difficult to meet when either continuous fibers or high fiber content are used in the composites.

In recent years, two new classes of HPFRCC have emerged. Ductal® has a high tensile strength of 12 MPa and a ductility of 0.02 to 0.06% (Chanvillard and Rigaud, 2003). Engineered cementitious composite (ECC), originally developed at the University of Michigan, has a typical moderate tensile strength of 4 to 6 MPa and a higher ductility of 3 to 5% (Fischer et al., 2003; Li, 1993). The tensile stress–strain curves of these two types of HPFRCCs are illustrated in Figure 24.2. The development approach for these two classes of materials is quite different. For Ductal®, which can be traced back to the work of Bache (1981),

the approach is to employ a tightly packed dense matrix to increase both tensile and compressive strength of the material. Fiber is added to counteract the resulting high brittleness of the densified matrix. The dense matrix allows a strong bond with the fiber that results in a high post-cracking strength as long as a fiber with high strength is utilized. For ECC, the approach is to create synergistic interactions between the fiber, matrix, and interface to maximize the tensile ductility through development of closely spaced multiple microcracks while minimizing the fiber content (generally 2% or less by volume). This approach is detailed in Section 24.2.3. Ductal® is designed for use in the elastic stage, so the fiber action becomes effective only when the structural ultimate limit state (ULS) is approached. ECC is generally designed for use in the elastic and strain-hardening (inelastic) stages, so fiber action becomes effective even under normal service loads. The development of ECC is still evolving, even though a number of full-scale structural applications have already appeared in Japan, Europe, and the United States. This chapter summarizes some basic knowledge of ECC. In the following, the fundamental characteristics of ECC are described. This is followed by a section on structural behavior of steel-reinforced ECC elements (R/ECC) and a section on the durability behavior of ECC material and R/ECC.

The literature on ECC is rapidly expanding with contributions from academic research and industrial organizations around the world. Some good sources of references include recent workshop or conference proceedings on this subject, such as HPFRCC in Structural Applications (Fischer and Li, 2006), FraMCoS-6 (Carpinteri et al., 2007), and HPFRCC 5 (Reinhardt and Naaman, 2007). These documents contain a number of papers on ECC and related subjects. To assist in the transition to broader industrial use, the Japan Society of Civil Engineers has published a design guideline (JSCE, 2007; Rokugo et al., 2007), and the RILEM TC HFC technical committee will be publishing two state-of-the-art reports on this subject. To aid the reader in maneuvering this literature, some clarification on semantics will be helpful. The name *engineered cementitious composite* (ECC) was adopted by the original developers (Li, 1993) to emphasize the micromechanics basis behind the design of this material. Micromechanics serves as a powerful tool to guide materials design for targeted composite properties and enables meaningful linkage between materials engineering and structure performance design (Li, 2007). In 2006, the RILEM TC HFC technical committee decided to emphasize the unique tensile strain-hardening response of this material (Figure 24.1) as a constitutive law for structural engineering design and gave the more descriptive name *strain-hardening cementitious composite* (SHCC) to this class of materials. The Japan Society of Civil Engineers, however, prefers to emphasize the multiple fine cracking (and associated durability; see Section 24.5), thus they refer to the material as *multiple fine cracking fiber-reinforced cementitious composite*. In essence, all of these materials are designed using micromechanical tools and represent identical material technology.

24.2 General Characteristics

24.2.1 The Family of ECC Materials

Engineered cementitious composite can be regarded as a family of materials with a range of tensile strengths and ductilities that can be adjusted depending on the demands of a particular structure. ECC also represents a family of materials with different functionalities in addition to the common characteristics of high tensile ductility and fine multiple cracking. Self-consolidating ECC (e.g., ECC M45 and its variants) is designed for large-scale, on-site construction applications (Kong et al., 2003; Lepech and Li, 2007). High-early-strength ECC (HES-ECC) is designed for applications that require rapid strength gain, such as transportation infrastructure that must be quickly reopened to the motorist public (Wang and Li, 2006a). Lightweight ECC (LW-ECC) is designed for applications where the dead load of structural members must be minimized (Wang and Li, 2003). Green ECC (G-ECC) is designed to maximize material greenness and infrastructure sustainability (Lepech et al., 2007; Li et al., 2004b). Self-healing ECC (SH-ECC) emphasizes the functionality of recovering transport and mechanical properties after experiencing damage (Li and Yang, 2007; Yang et al., 2005).

TABLE 24.1 Major Physical Properties of ECC

Compressive Strength (MPa)	First Crack Strength (MPa)	Ultimate Tensile Strength (MPa)	Ultimate Tensile Strain (%)	Young's Modulus (GPa)	Flexural Strength (MPa)	Density (g/cc)
20–95	3–7	4–12	1–8	18–34	10–30	0.95–2.3

Engineered cementitious composite using local material ingredients has been successfully produced in various countries, including Japan (Kanda et al., 2006a,b), Europe (Mechtcherine and Schulze, 2006), and South Africa (Boshoff and van Zijl, 2007), in addition to the United States. To successfully develop local versions of ECC, a good understanding of the underlying design approach is helpful (Kanda and Li, 1999; Li, 1993). A synopsis of the ECC design approach is given in Section 24.2.3.

A summary of major physical properties of ECC is given in Table 24.1. It should be emphasized that ECC properties can be tailored by the use of micromechanics tools. Even broader ranges of properties beyond those in this table can be expected in the future as the need arises. The very high strength and modulus version was attained by Kamal et al. (2007). The very high tensile ductility version was reported in Li et al. (1996). The super lightweight version was described in Wang and Li (2003). The common characteristic of these ECC materials is that they have tensile ductility orders of magnitude higher than those in typical concrete or FRC materials.

It should be noted that, although a large body of literature has developed around ECC based on polyvinyl alcohol fiber, commonly referred to as PVA-ECC, other fibers have been successfully utilized. These include high-modulus polyethylene (PE) fibers (Kamal et al., 2007; Li, 1993; Li and Wang, 2002) and polypropylene (PP) fibers (Takashima et al., 2003; Yang and Li, 2008). The principle behind the design of ECC, as discussed in Section 24.2.3, does not depend on a particular fiber. Fibers with certain properties, however, may meet the criteria for tensile strain hardening at a lower volume fraction. Decisions on what fibers to use will depend on their natural characteristics, including mechanical characteristics, diameter ranges, and surface characteristics; on the resulting ECC mechanical, durability, and sustainability performance; and on economics.

24.2.2 Tensile Characteristics

As indicated earlier, the most important characteristic of ECC is the high tensile ductility represented by a uniaxial tensile stress–strain curve with strain capacity as high as 5% (Figure 24.2b,c and Figure 24.3). This metal-like behavior shows a characteristic *yield point* at the end of the elastic stage when the first

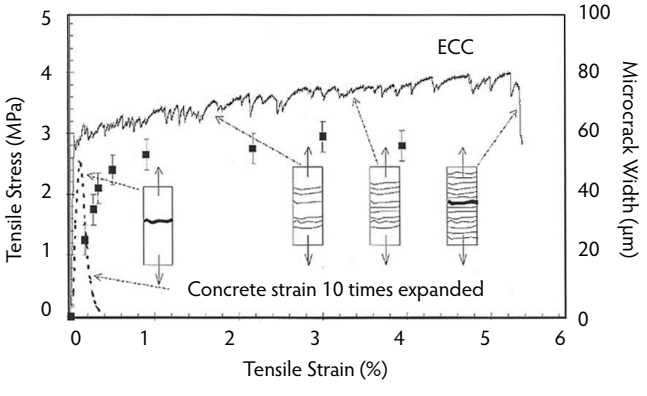

FIGURE 24.3 A tensile stress–strain curve of an ECC, showing also the crack width development (square symbols) as a function of imposed tensile strain.

microcrack appears on the specimen. Subsequent increase in load results in a strain-hardening response—that is, a rise in tensile deformation (volumetric straining in the form of multiple microcracking as opposed to localized crack opening) accompanied by a rise in load. Final failure of the specimen occurs when one of the multiple cracks forms a fracture plane. Beyond this peak load, ECC is no different than normal FRC, showing a tension-softening response. The high tensile ductility is of great value in enhancing the structural ultimate limit state (ULS) in terms of structural load and deformation capacity as well as energy absorption. In this manner, ECC can offer structural safety improvements. This contribution of ECC to structural response enhancement is discussed further in Section 24.4.

The formation of multiple microcracking is necessary to achieve high composite tensile ductility. Between first cracking strain (about 0.01%) and 1% strain, the microcrack opening increases from 0 to about 60 μm. Further loading beyond 1% causes more multiple cracks to form, but with no additional crack opening beyond the steady-state value of 60 μm (Figure 24.3). Governed by the mechanics of the fiber–matrix interaction within ECC, this unique characteristic is critically important for durability (see Section 24.5) of both material and structure. Unlike concrete or FRC, the steady-state crack width is an intrinsic material property, independent of loading (tension, bending, or shear), structure size and geometry, and steel reinforcement type and amount. This observation has important implications in service life, maximum member size, economics, and architectural aesthetics. In short, where steel reinforcement is used to control crack width in concrete, such steel reinforcement can be completely eliminated in ECC. By suppressing cracks with large crack width even in the presence of large imposed structural deformations, ECC can offer structural durability improvements in addition to watertightness and other serviceability enhancements. Although Figure 24.3 shows a particular example of ECC with steady-state crack width at 60 μm, even tighter crack widths, as low as 20 μm, have been achieved (Yang et al., 2007).

24.2.3 ECC Material Design Considerations

To attain high tensile ductility and tight microcrack width while keeping the fiber content low (2% or less by volume), ECC has been optimized through the use of micromechanics (Li, 1993; Li and Leung, 1992). Micromechanics is a branch of mechanics applied at the material constituent level that captures the mechanical interactions among the fiber, mortar matrix, and fiber–matrix interface. Typically, fibers are of the order of millimeters in length and tens of microns in diameter, and they may have a surface coating on the nanometer scale. Matrix heterogeneities in ECC, including defects, sand particles, cement grains, and mineral admixture particles, have size ranges from nano- to millimimeter scale. Ideally, the micromechanics model should capture all of the deformation mechanisms at the millimeter, micrometer, and nanometer scales; however, simplifying assumptions have been made to make the model equations tractable, and the resulting conditions (in closed-form solution) for strain hardening can be used as guidelines for material component tailoring. These conditions are expressed in strength and energy terms, as shown in Equation 24.1:

Strength criterion

$$\sigma_0 \geq \sigma_{cs} \tag{24.1a}$$

Energy criterion

$$J_b' \equiv \sigma_0 \delta_0 - \int_0^{\delta_0} \sigma(\delta) d\delta \geq J_{tip} \approx \frac{K_m^{\ 2}}{E_m} \tag{24.1b}$$

where σ_{cs} and σ_0 are the cracking strength and maximum fiber bridging capacity on each potential crack plane; δ_0 is the crack opening corresponding to σ_0 in the fiber bridging relationship $\sigma(\delta)$, which goes through a maximum; J_{tip} and J_b' are the crack tip matrix toughness and the complementary energy of the fiber bridging relation, respectively; and K_m and E_m are the matrix fracture toughness and Young's modulus, respectively. For derivation of Equation 24.1, see Li (1993). Physically, the strength criterion (Equation

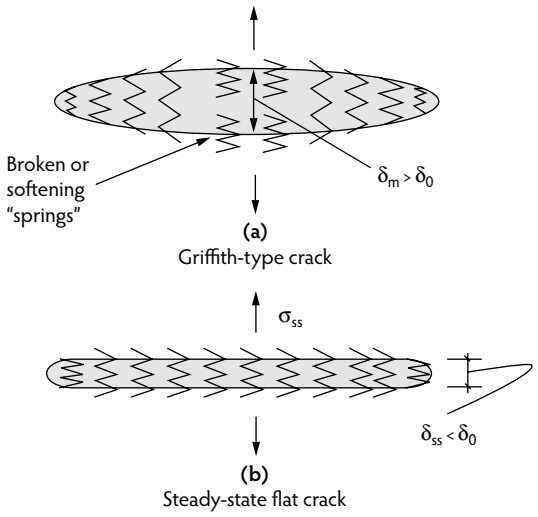

FIGURE 24.4 Illustration of the energy criterion for multiple cracking: (a) When Equation 24.1b is not satisfied, the common Griffith-type crack propagation results. Crack opening at the middle δ_m will exceed δ_0, causing spring failure and subsequent tension softening. (b) When Equation 24.1b is satisfied, the steady-state flat crack propagation mode prevails, with δ_{ss} staying below δ_0.

24.1a) ensures the initiation of microcracks from initial flaw sites in the composite before the tensile load exceeds the maximum fiber bridging capacity. The left-hand side of Equation 24.1a can be thought of as the maximum tensile load carried by a line of springs with tensile strength determined by the bridging fibers. Failure of the fiber springs is associated with fiber rupture, slippage, or pullout. Ensuring that the maximum fiber bridging capacities on existing crack planes remain higher than the matrix cracking strength of potential new crack planes allows additional cracks to form; otherwise, saturated multiple cracking would not be attained, and sparsely spaced cracks will result, limiting the tensile ductility.

The energy criterion (Equation 24.1b) prescribes the mode of crack propagation once initiated. The normal form of Griffith cracking is not favorable to multiple cracking. This is because the crack opening in Griffith-type cracks, especially at the midpoint of the crack line (δ_m), always increases with the length of the crack, and failure of the bridging fiber invariably results, either in the form of fiber pullout or breakage beginning at this widest point when δ_m exceeds δ_0. The only means of preventing this is by altering the Griffith crack propagation mode to a flat crack propagation mode whereby the crack extends while the crack opening remains constant at any location (apart from a small bridging zone near the crack tip) regardless of the length of the crack. In this manner, δ_m stays below δ_0 along the entire crack line. During flat crack propagation, energy is exchanged between work input (from applied loading) and energy absorbed by the fiber bridging process in the opening of the crack near the crack tip (and only near the crack tip), as well as matrix material breakdown at the crack tip. The enforcement of energy balance results in Equation 24.1b. Violation of Equation 24.1b results in fracture localization, as in the case of FRC, and terminates the multiple cracking process. The energy criterion is illustrated in Figure 24.4.

It should be noted that both parts of Equation 24.1 have been arranged so the left-hand sides of the inequality sign contain terms that pertain to fiber and interface properties, while the right-hand sides contain terms that pertain to matrix properties, all of which are measurable physical properties. This observation emphasizes the usefulness of Equation 24.1 to aid in the fiber, matrix, and interface selection or tailoring process to arrive at viable compositions of ECCs. As an example, this approach has been adopted for tailoring of the surface coating on PVA fibers (Li et al., 2002) and for the deliberate introduction of matrix defects in lightweight ECC (Wang and Li, 2003) and high-early-strength ECC (Wang and Li, 2006a). The equality signs in Equation 24.1 are based on the assumption that initial defect size and fiber volume fraction are uniform throughout the composite. In reality, variability of these

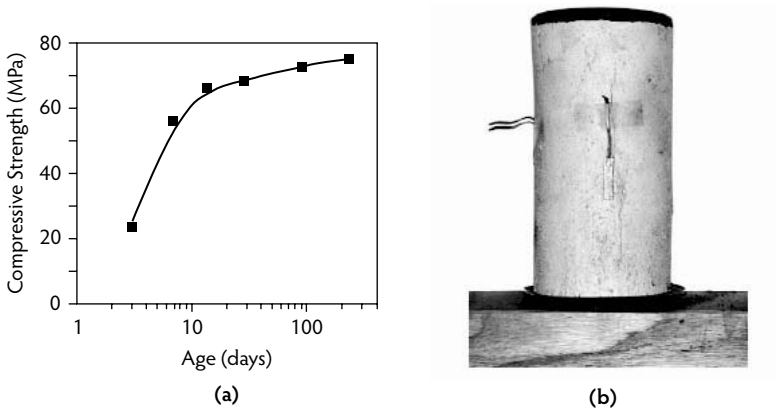

FIGURE 24.5 (a) Compressive strength development of ECC (M45), and (b) ECC specimen after compressive strength test. (From Wang, S. and Li, V.C., in *Proceedings, High-Performance Fiber-Reinforced Cementitious Composites (HPFRCC) in Structural Applications*, Fischer, G. and Li, V.C., Eds., RILEM, Paris, 2006, pp. 65–73.)

parameters must exist and depends on the mix composition as well as mixing procedure. This variability creates the need for a wider margin between the left- and right-hand sides of Equation 24.1 and explains the use of the inequality signs. Kanda and Li (2006) specifically studied the necessary margin to create robust tensile properties.

24.2.4 Compressive and Flexural Characteristics

The compressive properties of ECC are not significantly different from normal- to high-strength concrete. Compressive strengths of ECC range from 20 to 95 MPa. The elastic modulus of 15 to 34 GPa is typically lower than that for concrete due to the absence of coarse aggregates. The compressive strain capacity of ECC is slightly higher, around 0.45 to 0.65%. Figure 24.5a shows a strength development curve for an ECC (M45) compressive cylinder. The post-peak behavior of ECC under compression tends to descend more gently than high-strength concrete, accompanied by a gradual bulging of the specimen (Figure 24.5b) rather than explosive crushing failure. The flexural response of ECC reflects its tensile ductility (Kunieda and Rokugo, 2006a; Maalej and Li, 1994; Wang, 2005; Wang and Li, 2006). Under bending, multiple microcracking forms at the base of the beam, allowing it to undergo a large curvature development, a phenomenon that has resulted in the popular name of *bendable concrete*. A flexural strength (modulus of rupture, or MOR) of 10 to 15 MPa is easily achievable and is accompanied by a significant deflection-hardening regime (Figure 24.6a). Deflection hardening is an intrinsic property of ECC that does not depend on geometry. This is not the case for tension-softening FRC, for which deflection hardening becomes more difficult to attain as beam height increases (Stang and Li, 2004). A highly deformed ECC beam and fine multiple cracking on the tensile side of the beam are shown in Figure 24.6b,c (Wang, 2005; Wang and Li, 2006b). Engineered cementitious composite has significant improvements in fatigue response over normal concrete and FRC. Suthiwarapirak et al. (2002) conducted flexural fatigue tests on ECC and demonstrated higher ductility and fatigue life compared with polymer cement mortars commonly used in repair applications.

24.3 Mixture Proportioning, Material Processing, and Quality Control

Table 24.2 gives a typical mix design for ECC (ECC-M45) with self-consolidating casting properties. All proportions are given with materials in the dry state. The ingredients and mix proportions have been optimized to satisfy the multiple cracking criteria (Equation 24.1). Specifically, the type, size, and amount of fiber and matrix ingredients, along with interface characteristics, are tailored for multiple cracking

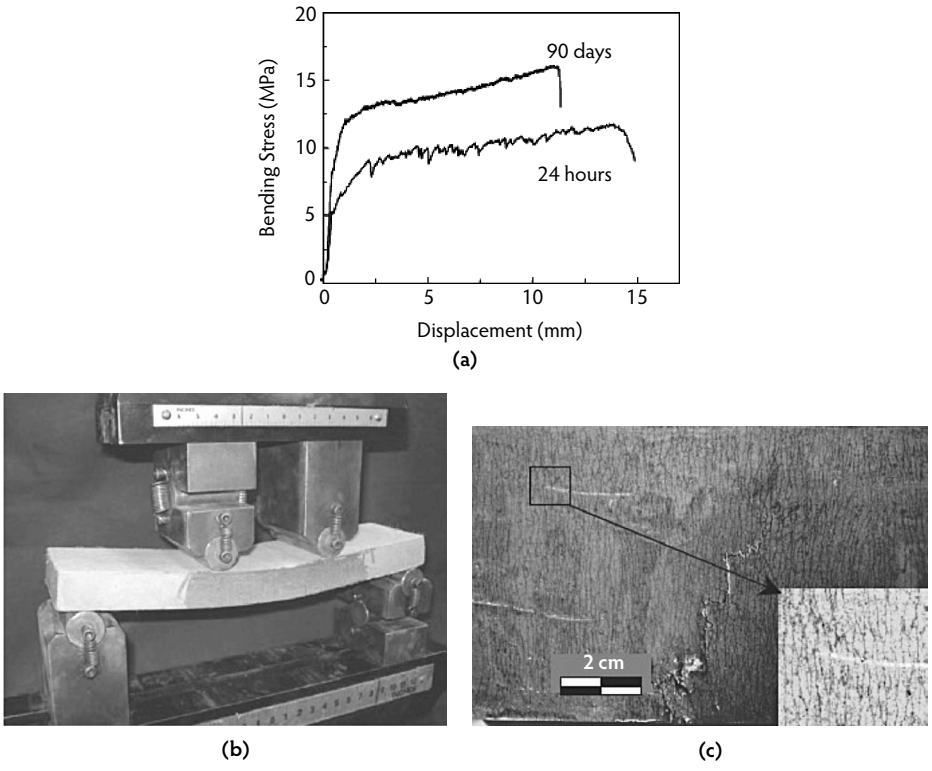

FIGURE 24.6 (a) Flexural load–deflection curve of an ECC, (b) ECC flexural specimen showing large deflection, and (c) fine multiple cracking on the tensile side of beam 304 mm (length) × 76.2 mm (width) × 25.4 mm (depth). (Adapted from Wang, S. and Li, V.C., in *Proceedings, High-Performance Fiber-Reinforced Cementitious Composites (HPFRCC) in Structural Applications*, Fischer, G. and Li, V.C., Eds., RILEM, Paris, 2006, pp. 65–73.)

and controlled crack width. ECC incorporates fine silica sand with a sand/binder ratio (S/B) of 0.36 to maintain adequate stiffness and volume stability. ECC-M45 has a water/binder (w/b) ratio of 0.26 to attain a good balance of fresh and hardened properties. The binder system is defined as the total amount of cementitious material (i.e., cement and fly ash, Type F) in ECC. The silica sand has a maximum grain size of 250 μm and a mean size of 110 μm. The aggregated particle size of all matrix components should be properly graded to achieve self-consolidating fresh properties (Fischer et al., 2003).

Various fiber types have been used in the production of ECC, but ECC-M45, which currently has the largest experimental dataset, uses polyvinyl alcohol (PVA) fiber 12 mm in length and 39 μm in diameter. The nominal tensile strength, stiffness, and density of the fiber are 1600 MPa, 40 GPa, and 1300 kg/m^3, respectively. The PVA fiber is surface coated by a proprietary oiling agent (1.2% by weight) to reduce the fiber–matrix interfacial bonding. To account for material heterogeneity, a fiber content of 2% by volume, which is greater than the calculated critical fiber content required to achieve strain hardening, is typically used in the mix design. The mix design described above has been experimentally demonstrated in a broad range of investigations to consistently produce good ECC fresh and hardened properties. A high-range

TABLE 24.2 Engineered Cementitious Composite Mix Design Proportions by Weight for ECC-M45

Mix Designation	Cement	Fly Ash	Sand	Water	High-Range Water Reducer (HRWR)	Fiber (Vol. %)
M45	1.0	1.2	0.8	0.56	0.012	0.02

TABLE 24.3 Material Charging Sequence into Ready-Mix Trucks

Activity No.	Activity	Elapsed Time (min)
1	Charge all sand.	2
2	Charge approximately 90–95% of mixing water, all HRWR, all hydration stabilizer.	2
3	Charge all fly ash.	2
4	Charge all cement.	2
5	Charge remaining mixing water to wash drum fins.	4
6	Mix at high RPM for 5 minutes or until material is homogenous.	5
7	Charge fibers.	2
8	Mix at high RPM for 5 minutes or until material is homogenous.	5
	Total	24

water-reducing (HRWR) admixture containing a polycarboxylate chemical composition has been found to be most effective in maintaining the desired fresh property during mixing and placing. Adaptations of this reference mix have been used in various construction projects. Full-scale production of ECC was carried out in Japan (Kunieda and Rokugo, 2006b) and in the United States (Lepech and Li, 2007). Experience in concrete ready-mix plants suggests the charging sequence of raw material shown in Table 24.3.

The properly mixed ECC material should have a creamy texture, as shown in Figure 24.7. To ensure good self-consolidation behavior, the deformability of ECC in the fresh state should be checked at the construction site. To perform this check, a standard concrete slump cone is filled with fresh ECC material and emptied onto a level Plexiglas® or glass plate. The flowable ECC material flattens into a large pancake-shaped mass (Figure 24.8a). Two orthogonal diameters of this "pancake" are measured, and a characteristic deformability factor, denoted by Γ, is calculated:

$$\Gamma = \frac{\left(D_1 - D_0\right)}{D_0} \tag{24.2}$$

where D_1 is the average of two orthogonal diameter measurements after slump cone removal, and D_0 is the diameter of the bottom of the slump cone. For good self-consolidation, Γ should have a minimum value of 2.75 (Lepech and Li, 2007). Excessively large values of Γ, however, may indicate improper mix proportions, may potentially result in component segregation, and must be avoided. Typically, the

FIGURE 24.7 Creamy texture appearance of fresh ECC in mixing drum of a ready-mix truck. (From Lepech, M.D. and Li, V.C., *ACI Mater. J.*, 2008.)

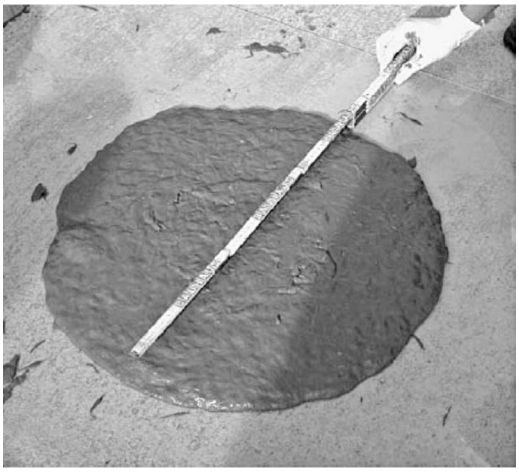

(a)

(b)

FIGURE 24.8 (a) Slump cone test of ECC flowability; (b) Marsh cone flow rate test.

deformability value decreases over time during mixing and transport in the ready-mix concrete truck. The use of a hydration stabilizer has been found effective in maintaining good deformability without negatively affecting the hardened properties. To minimize the danger of early-age cracking, wet curing for a minimum of 7 days and nighttime casting of field applications are recommended for ECC when the air temperature is above 50°F.

Care must be taken to ensure good fiber dispersion in the mix. Yang et al. (2007) found that an effective means of controlling fiber dispersion is to ensure good mortar viscosity via a Marsh flow cone test. In the Marsh cone flow test, the funnel is filled completely with mortar (ECC mortar without fibers), and the bottom outlet is then opened, allowing the mortar to flow (Figure 24.8b). The Marsh cone flow time of mortar is the elapsed time in seconds between the opening of the bottom outlet and the time when light becomes visible at the bottom, when observed from the top.

In addition to the standard compression cylinder test typically applied to concrete quality control on job sites, the tensile coupon test should also be carried out to ensure that the tensile properties specified in design documents are met. These compression and tensile tests should be conducted at the ages of 4

days, 7 days, 14 days, and 28 days to observe property development over time. It is recognized that uniaxial tension tests are difficult to carry out on a routine quality control basis. As a result, a simpler bending test accompanied by inversion schemes to obtain material tensile properties is being developed (Kanakubo, 2006; Qian and Li, 2007).

Apart from ready-mix and self-consolidating casting, special versions of ECC have also been developed for extrusion (Stang and Li, 1999) and shotcreting (Kanda et al., 2001; Kim et al., 2003; Kojima et al., 2004). Precasting of ECC structural elements has been utilized for coupling beams in high-rise buildings in Japan (Kanda et al., 2006a,b). Kanda et al. concluded that full-scale production in a precast plant of ECC with high mechanical performance and excellent fluidity is achievable in practice. Figure 24.9 shows the various methods of ECC material processing. Although these ECC materials all carry the same hardened material characteristics described in Section 24.2, they exhibit significantly different fresh properties to meet different processing requirements. The relatively small amount of fibers used in ECC allows such versatility in processing methods.

24.4 Behavior of ECC Structural Elements

A variety of experiment programs have been performed to assess the performance of ECC at the structural element level for both seismic and non-seismic structural applications (Table 24.4). These experiments provide insight into how unique ECC material properties elevate the response performance of the structure. Within this section, we describe some observed responses of elements subjected to monotonic and fatigue flexural loading, cyclic shear loading, and steel–ECC interactions. Fundamental knowledge will then be drawn from these studies.

24.4.1 Structural Response of R/ECC Elements

24.4.1.1 Flexural Elements

Fischer and Li (2002a) studied the behavior of R/ECC flexural elements under reversed cyclic loading. The test setup is shown in Figure 24.10, and the specimen configuration is shown in Figure 24.11. A regular reinforced-concrete (R/C) beam was also tested as control. Figure 24.12 shows the substantial difference in hysteretic response for the R/ECC and the R/C control column specimens. A significantly fuller hysteretic loop with larger energy dissipation was achieved by the R/ECC beam despite the fact that no shear stirrups were used at the base of the flexural element. The damage experienced by these elements at 10% interstory drift is compared in Figure 24.13. Even at this high drift level, no spalling of the ECC was observed. In contrast, the R/C column lost all concrete cover near the fixed end subsequent to bond splitting and spalling. Clearly, the R/ECC element demonstrated significant damage tolerance under severe loading.

The high cycle fatigue response of R/ECC flexural elements was studied by Kim et al. (2004) in conjunction with a bridge deck link slab application. The full-thickness slab test configuration is provided in Figure 24.14, which shows the steel girder (anchored to the slab by steel studs) on top for convenience of testing. Over 100,000 cycles, no degradation in stiffness was observed in the R/ECC or in the R/C control beam; however, the cracks in the R/C beam grew continuously to 0.6 mm at the end of the test, while the microcracks in R/ECC beam remained at approximately 50 μm (Figure 24.15).

Motivated by the need to increase the stiffness and to reduce the tendency for fatigue cracking in steel bridge decks, a steel/ECC composite beam was studied by Walter et al. (2004) under monotonic flexural loading (Figure 24.16). For control, a steel/FRC and a steel/FRD composite beam were also tested in the same configuration. FRD is a fiber-reinforced Densit® material, a very high strength and dense concrete reinforced with steel fibers similar to Ductal®. All concrete materials were cast onto the steel plate and bonded only by adhesion to the roughened steel surface. The load-deflection response captured in Figure 24.17 demonstrates a much higher load capacity in the case of the steel/ECC beam, which showed multiple microcracking during testing, suppressing the formation of a brittle fracture that limits the capacity of the steel/concrete beam. The single fracture in the FRC and FRD beams led to their immediate debonding from the steel plate.

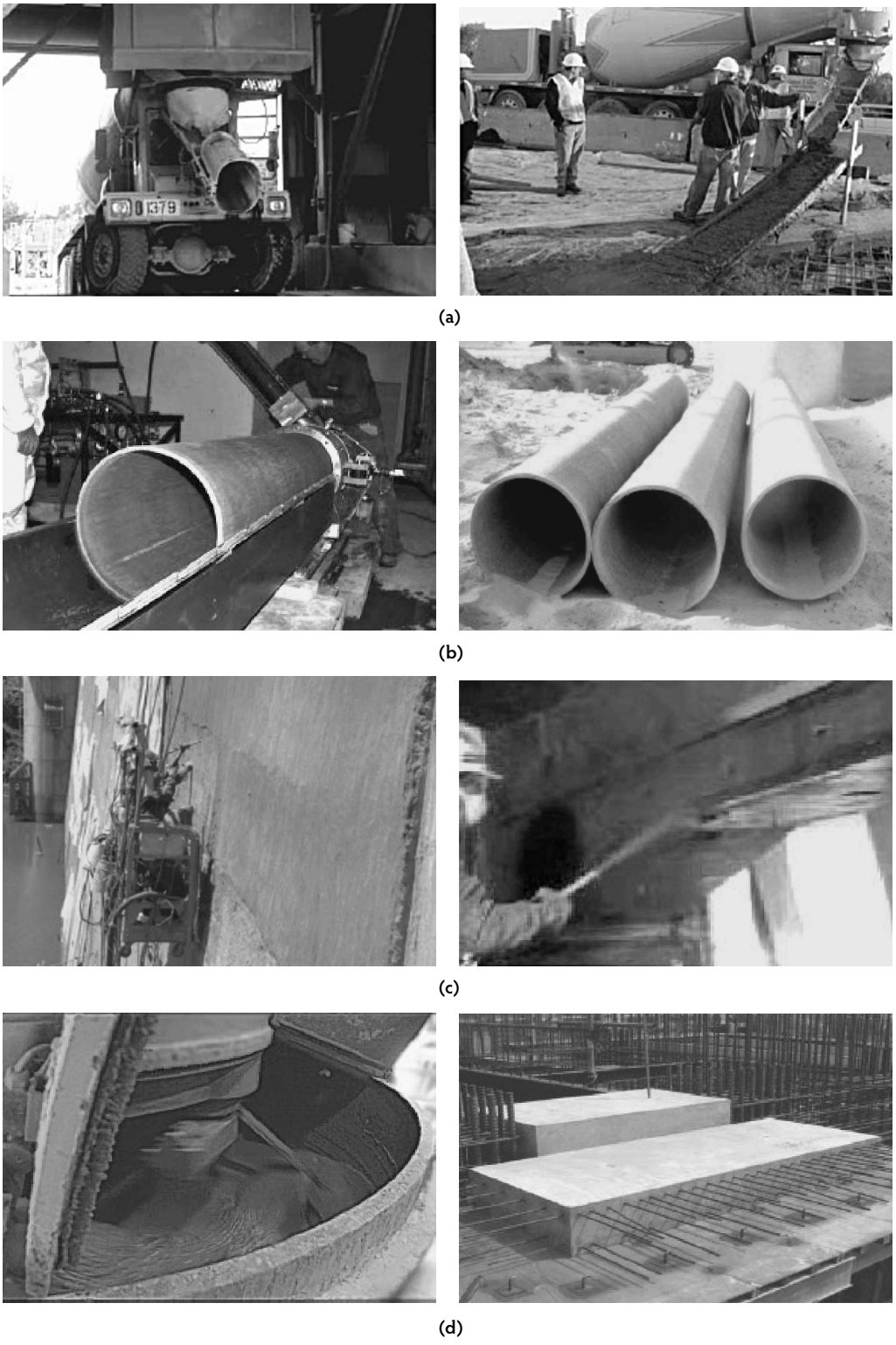

FIGURE 24.9 Various processing methods of ECC: (a) self-consolidating casting, (b) extrusion, (c) spraying, (d) precast mixing (photograph courtesy of S. Staniski) and precasted element.

TABLE 24.4 A Summary of Various R/ECC Structural Elements Previously Studied

Structural Element Type	Type of Loading (Type of Reinforcement)[a]	Refs.
Flexural elements	Reversed cyclic	Fischer and Li (2002a)
	Monotonic (GFRP)	Li and Wang (2002)
	Reversed cyclic (CFRP)	Fischer and Li (2003a)
	Fatigue	Kim et al. (2004)
Column elements	Reversed cyclic	Fukuyama et al. (2000)
Shear beam elements	Reversed cyclic	Kanda et al. (1998)
	Reversed cyclic	Fukuyama et al. (2000)
	Monotonic	Shimizu et al. (2006)
	Monotonic	Kabele and Kanakubo (2007)
Beam–column connections	Reversed cyclic	Parra-Montesinos and Wight (2000)
Wall elements	Repeated shear	Kanda et al. (1998)
	Reversed cyclic	Kesner and Billington (2005)
	Reversed cyclic	Fukuyama et al. (2006)
Frames	Reversed cyclic (steel and CFRP)	Fischer and Li (2003b)
Steel/ECC interactions	Monotonic flexure (plate/ECC)	Walter et al. (2004)
	Monotonic shear (stud/ECC)	Qian and Li (2006)
	Monotonic tension (anchor/ECC)	Leung et al. (2006); Qian (2007)

[a] Steel reinforcement unless specified.

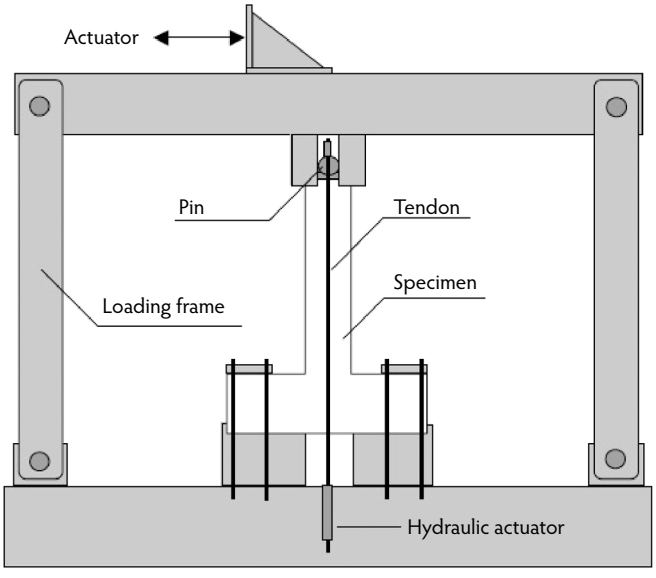

FIGURE 24.10 Test setup for full reversed loading of flexural elements. (From Fischer, G. and Li, V.C., *ACI Struct. J.*, 99(6), 781–790, 2002.)

24.4.1.2 Shear Element

Fukuyama et al. (2000) studied the behavior of R/ECC shear elements under reversed cyclic loading. The specimen configuration is shown in Figure 24.18, and the hysteretic loops for R/ECC and R/C are shown in Figure 24.19. Again, the hysteretic loops for R/ECC showed much greater stability and ability to dissipate energy. The R/C specimen suffered extensive bond splitting and loss of cover, accompanied by large diagonal cracks. In contrast, the damage experienced by the R/ECC shear element was significantly lower (Figure 24.20). No bond splitting or cover loss was observed, and microcracks continued to carry

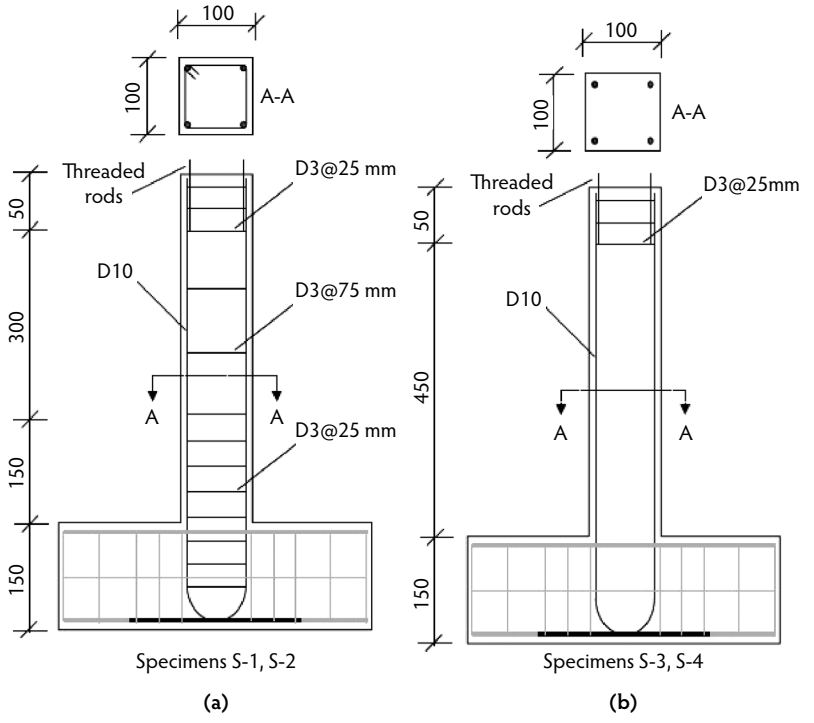

FIGURE 24.11 Specimen configurations of flexural elements: (a) R/C; (b) R/ECC with no stirrups in shear zone. (From Fischer, G. and Li, V.C., *ACI Struct. J.*, 99(6), 781–790, 2002.)

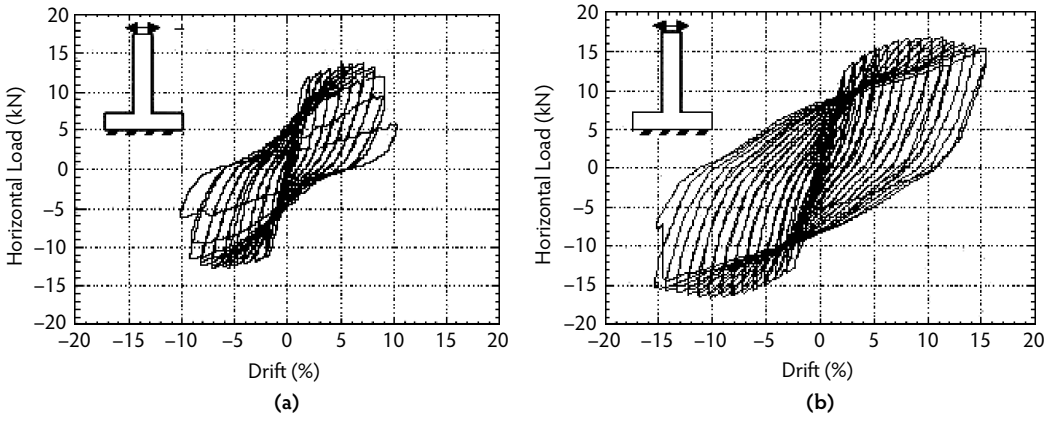

FIGURE 24.12 Hysteretic behavior of flexural members under fully reversed cyclic loading for (a) R/C with stirrups, and (b) R/ECC without stirrups. (From Fischer, G. and Li, V.C., *ACI Struct. J.*, 99(6), 781–790, 2002.)

loads up to a 5% rad deflection angle. The shear capacity of a R/ECC beam can be estimated from a linear superposition of the contributions of the ECC material and the shear and axial steel reinforcements due to the compatible deformation of the two materials even after steel yields. This approach was suggested to be reasonably accurate and conservative (Rokugo et al., 2007); however, numerical analysis combined with experimental data (Kabele and Kanakubo, 2007) suggested that only a fraction of the tensile strength and strain capacity of ECC might be utilized in the shear element due to possible damage of bridging fibers on sliding crack surfaces.

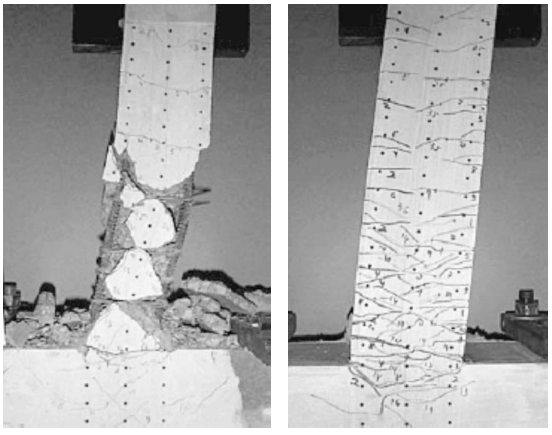

FIGURE 24.13 Damage behavior of (a) R/C and (b) R/ECC without stirrups, shown at 10% drift. (From Fischer, G. and Li, V.C., *ACI Struct. J.*, 99(6), 781–790, 2002.)

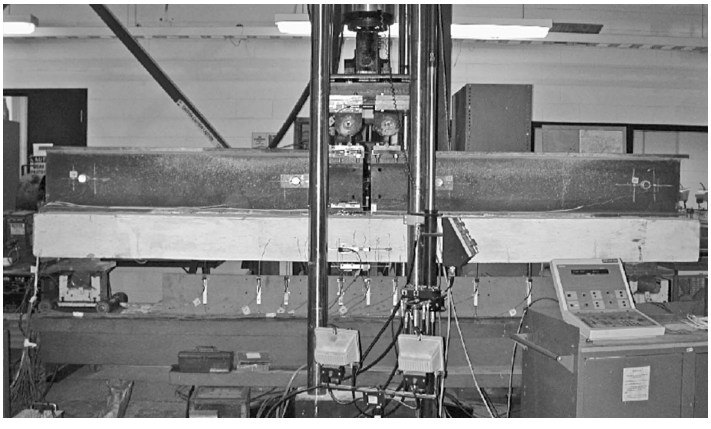

FIGURE 24.14 Flexural fatigue testing of ECC link-slab element. (From Kim, Y.Y. et al., *ACI Struct. J.*, 101(6), 792–801, 2004.)

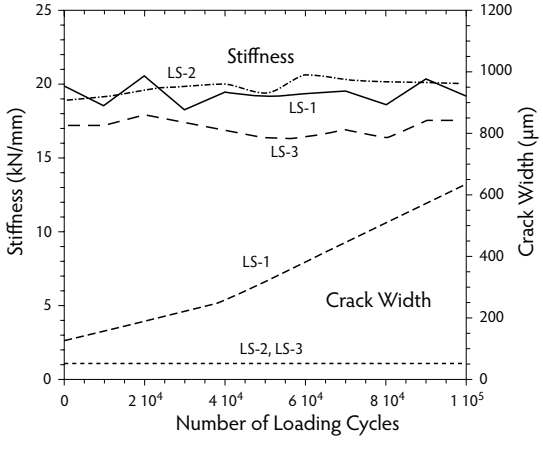

FIGURE 24.15 Stiffness and crack width change as a function of load cycles. LS-1 is the control R/C specimen; LS-2 and LS-3 are both R/ECC specimens with different reinforcement details to represent new and retrofit construction conditions. (From Kim, Y.Y. et al., *ACI Struct. J.*, 101(6), 792–801, 2004.)

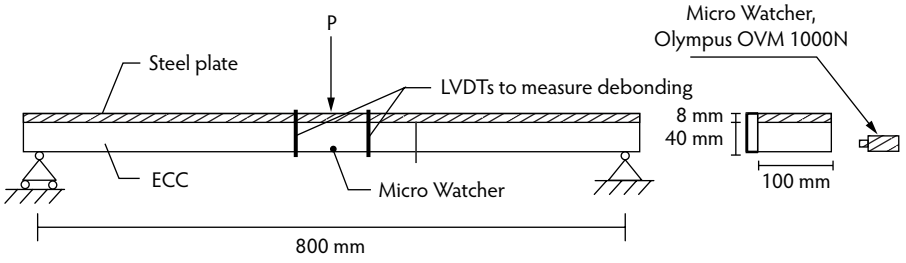

FIGURE 24.16 Composite steel/ECC beam test setup. (From Walter, R. et al., in *Proceedings of the 5th International PhD Symposium in Civil Engineering*, June 17–19, Delft, the Netherlands, 2004, pp. 477–484.)

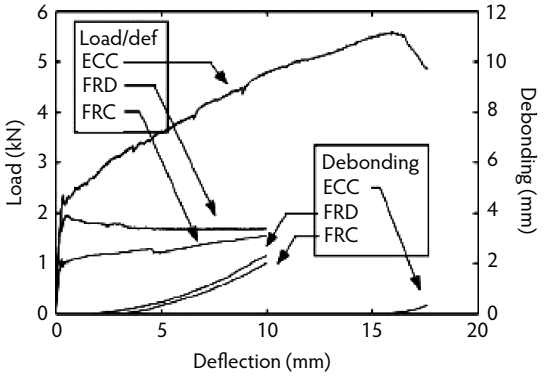

FIGURE 24.17 Load and debonding as a function of composite beam deflection. A significant increase in load capacity and a delay in debonding were achieved in the steel/ECC beam vs. the steel/FRC and steel/FRD beams. (From Walter, R. et al., in *Proceedings of the 5th International PhD Symposium in Civil Engineering*, June 17–19, Delft, the Netherlands, 2004, pp. 477–484.)

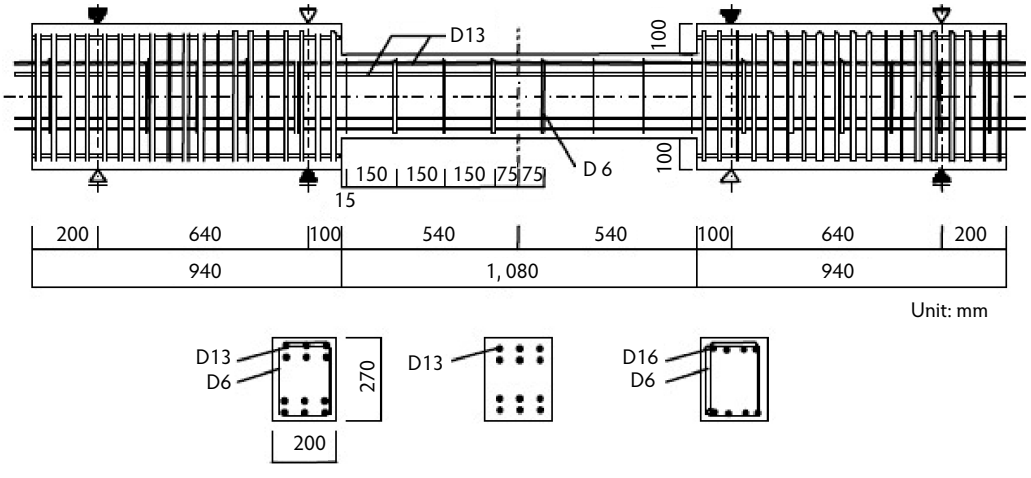

FIGURE 24.18 Fully reversed Ohno shear test setup. (From Fukuyama, H. et al., in *Proceedings of the 6th ASCCS International Conference on Steel–Concrete Composite Structures*, March 22–24, Los Angeles, CA, pp. 969–976.)

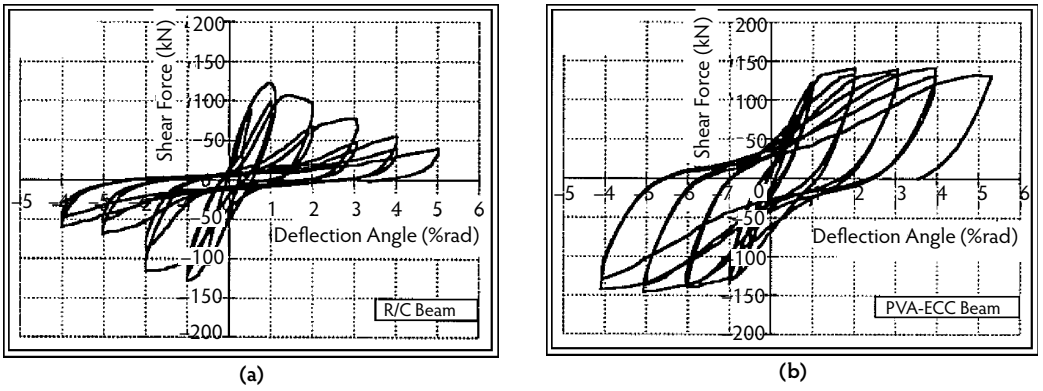

FIGURE 24.19 Hysteretic loops for Ohno shear beams under fully reversed cyclic loading for (a) R/C and (b) R/ECC. (From Fukuyama, H. et al., in *Proceedings of the 6th ASCCS International Conference on Steel–Concrete Composite Structures*, March 22–24, Los Angeles, CA, pp. 969–976.)

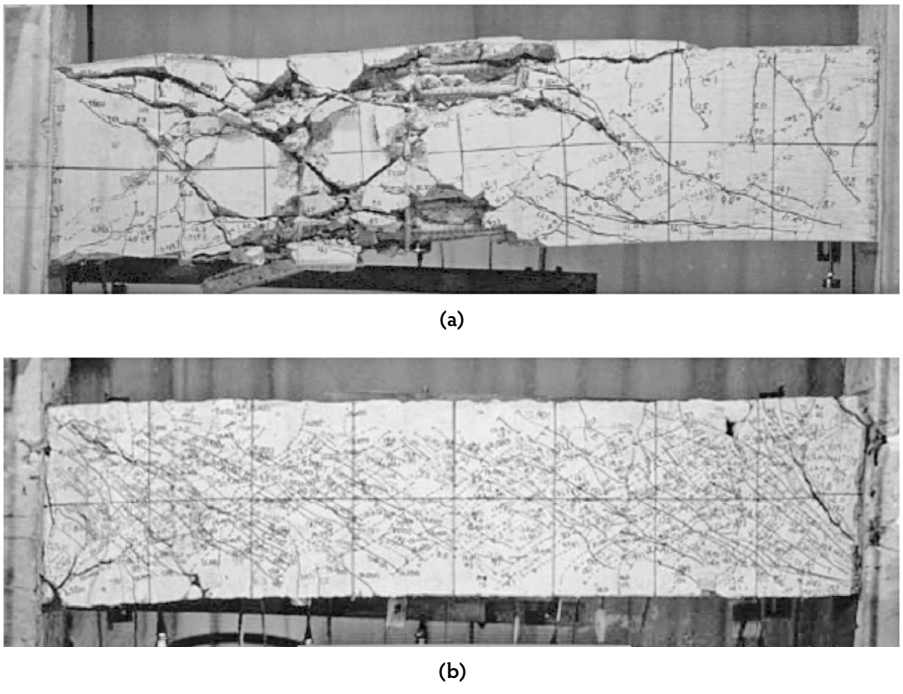

FIGURE 24.20 Damage pattern in Ohno shear beams: (a) R/C, and (b) R/ECC. (From Fukuyama, H. et al., in *Proceedings of the 6th ASCCS International Conference on Steel–Concrete Composite Structures*, March 22–24, Los Angeles, CA, pp. 969–976.)

24.4.1.3 Column Element

The response of R/ECC and R/C columns under fully reversed cyclic loading was studied by Fukuyama et al. (2000). These columns were tested under the antisymmetrical moment condition. The axial force applied to the column was 20% of the axial compressive strength of the column, calculated without the contribution of the steel reinforcements. The hysteretic behavior in terms of stability and energy dissipation was improved in the R/ECC column over the R/C column in a manner similar to that for flexural and shear elements (Figure 24.21). Large bond splitting cracks were observed in the R/C column, which

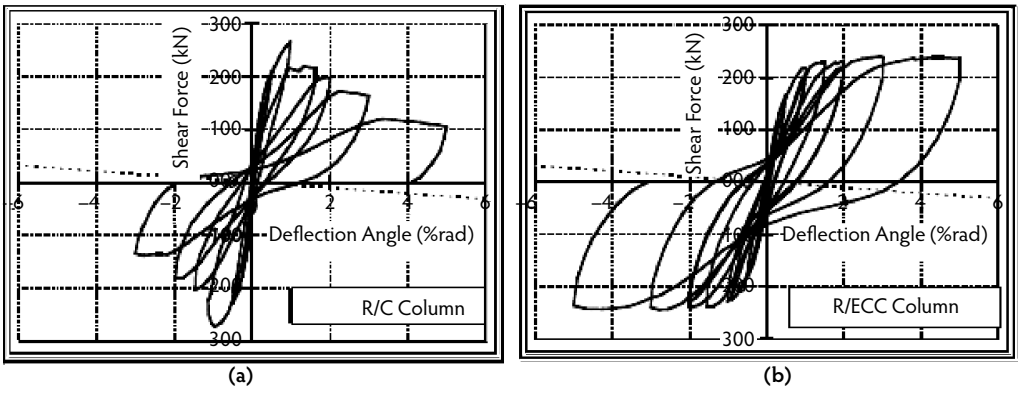

FIGURE 24.21 Hysteretic behavior of columns under fully reversed cyclic loading for (a) R/C and (b) R/ECC. (From Fukuyama, H. et al., in *Proceedings of the 6th ASCCS International Conference on Steel–Concrete Composite Structures*, March 22–24, Los Angeles, CA, pp. 969–976.)

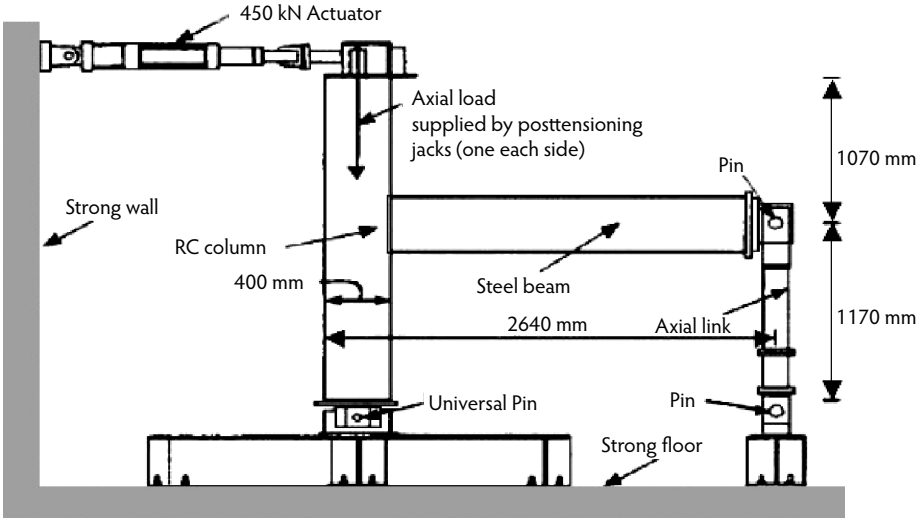

FIGURE 24.22 Test setup for beam–column connection. (From Parra-Montesinos, G. and Wight, J.K., *ASCE J. Struct. Eng.*, 126(10), 1113–1121, 2000.)

failed by shear without yielding of the longitudinal reinforcements; subsequently, the resistant shear force in the envelope curve of shear force–deflection angle relationship decreased with increase of deflection angle. On the other hand, the R/ECC column did not fail by shear or bond splitting. Instead, it maintained a ductile response up to the end of the test with fine cracks revealed on the specimen surface.

24.4.1.4 Beam–Column Connection Element

Beam–column connection was studied by Parra-Montesinos and Wight (2000), using the test setup shown in Figure 24.22. The hysteretic response for the R/ECC shear panel was substantially improved over the R/C (Figure 24.23), even when all shear stirrups were removed in the R/ECC shear panel. Under fully reversed cyclic loading, a set of orthogonal cracks formed in both specimens (Figure 24.24). Although the orthogonal cracks in R/ECC were much more closely spaced, they did not lead to surface spalling as is often observed in R/C specimens after large load reversals. In addition, edge spalling was revealed in the R/C specimen, associated with the bearing of the steel beam on the brittle concrete. This was not found in the R/ECC specimen.

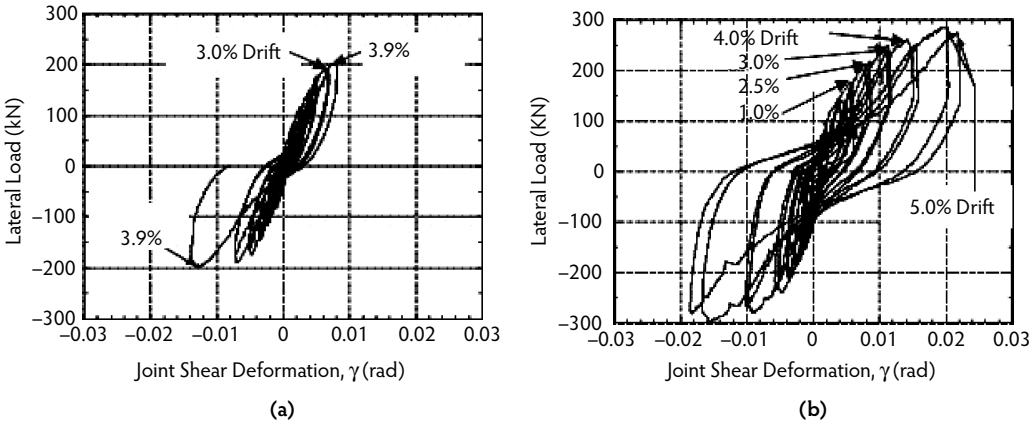

FIGURE 24.23 Hysteretic loops of fully reversed cyclic test on beam–column connections for (a) R/C with stirrups and (b) R/ECC without stirrups (From Parra-Montesinos, G. and Wight, J.K., *ASCE J. Struct. Eng.*, 126(10), 1113–1121, 2000.)

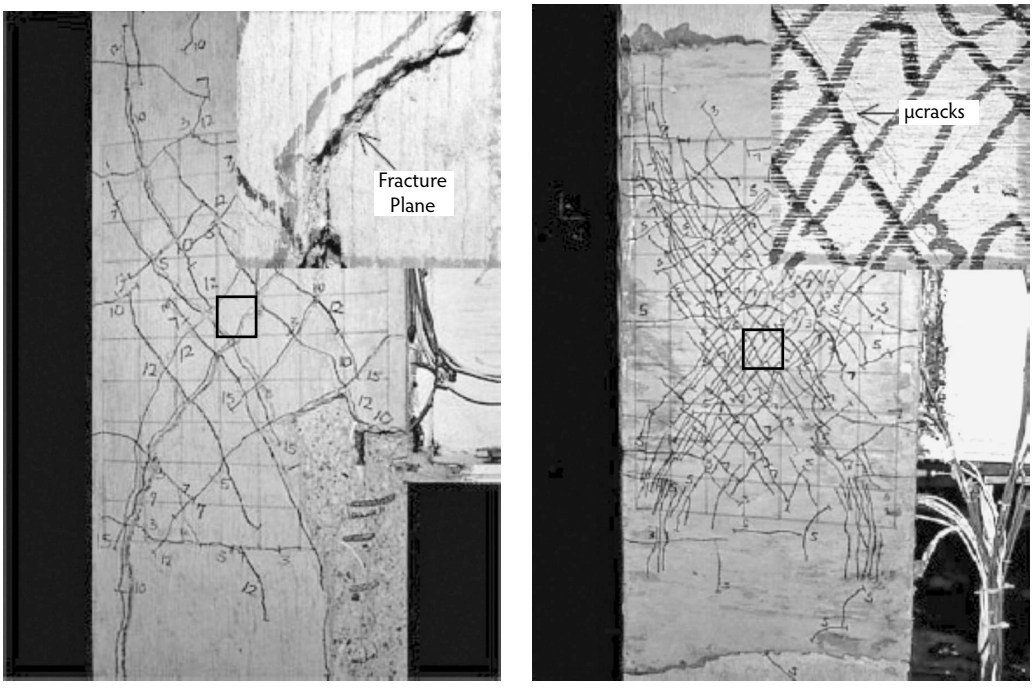

FIGURE 24.24 Damage behavior of the shear panel of a hybrid connection after cyclic loading. The enlarged inserts provide easier viewing of the cracks in (a) R/C and (b) R/ECC. (Adapted from Parra-Montesinos, G. and Wight, J.K., *ASCE J. Struct. Eng.*, 126(10), 1113–1121, 2000.)

24.4.1.5 Wall Panel Element

Wall panel elements were studied by Kesner and Billington (2005) under fully reversed cyclic loading, using the test setup shown in Figure 24.25. These tests confirmed that the R/ECC wall panels outperformed the R/C wall panels in hysteretic loop stability, peak load, and energy dissipation (Figure 24.26).

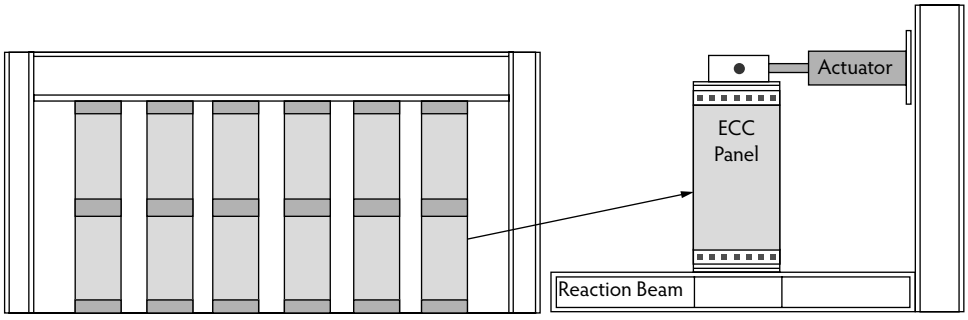

FIGURE 24.25 Wall panel test setup. (From Kesner, K.E. and Billington, S.L., *ASCE J. Struct. Eng.*, 131(11), 712–720, 2005.)

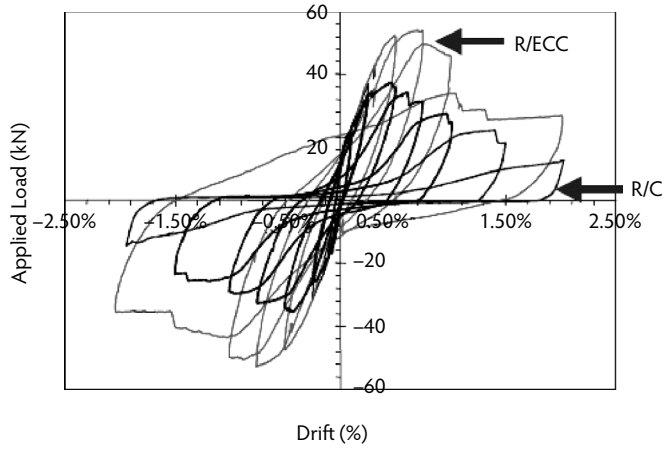

FIGURE 24.26 Hysteretic loops of shear wall. (Adapted from Kesner, K.E. and Billington, S.L., *ASCE J. Struct. Eng.*, 131(11), 712–720, 2005.)

24.4.2 Insights from R/ECC Element Response

The structural element experimental testing results briefly summarized in Section 24.4.1 share the common features of enhanced element load and deformation capacity, hysteretic loop stability, and energy dissipation. Further, structural damage is limited to microcracking while large fractures in the form of bond splitting and spalling are suppressed. A number of helpful insights for structural use of ECC can be drawn from the above studies. These are summarized below.

24.4.2.1 Potential for Reduction or Elimination of Shear Reinforcement

Through the formation of multiple cracks and delay of fracture localization, the ductility of R/ECC elements can be maintained with little or no conventional shear reinforcement. This is best demonstrated in the flexural element (Fischer and Li, 2002a) (Figure 24.11) and beam–column connection (Parra-Montesinos and Wight, 2000) studies highlighted in the previous section, where shear stirrups were completely eliminated. Additional evidence can be found in a study by Li and Wang (2002), who experimentally demonstrated that ECC beams without shear reinforcement exhibited superior performance compared to high-strength concrete beams with closely spaced steel stirrups. Experiments on the cyclic response of unbonded post-tensioned precast columns with ECC hinge zones (Billington and Yoon, 2004) also confirmed that column integrity could be better maintained when concrete is replaced by ECC without any seismic shear detailing.

24.4.2.2 Damage Tolerance

Damage tolerance is a measure of the residual strength of a material or structure when damage is introduced. The damage tolerance of ECC derives from the fact that fracture or real cracks are suppressed in favor of plastic yielding of ECC in the form of multiple microcracks. Such microcracks are not real cracks (Li, 2000) in the sense that an increasing amount of load can be carried across them during ECC strain hardening. Cracks in normal concrete or even in standard fiber-reinforced concrete are accompanied by tension softening, and load-carrying capacity drops as the crack enlarges. As a result, a reliance on steel reinforcement to maintain structural integrity becomes critical. Where no steel reinforcement exists (e.g., in the concrete cover), surface spalling results. Such failure modes are fully eliminated in R/ECC elements, as can be observed in Figure 24.13, Figure 24.20, and Figure 24.24. In these elements, the shear stiffness and the peak load at each load cycle are better maintained than in R/C due to the high damage tolerance of ECC. In structural elements loaded beyond first crack, it is reasonable to expect equal or even higher structural stiffness in R/ECC elements compared to R/C elements, despite the lower elastic modulus of ECC as compared to concrete. This is due to the capability of ECC to continue to share the load-carrying function with steel reinforcements, long after the first crack appears. This concept was verified in an analytic study of cracked reinforced beams by Szerszen et al. (2006). Fukuyama et al. (2007) regarded such damage tolerance functionality of ECC as a significant benefit to society, given the enormous economic cost of repair and reconstruction of infrastructures after a major seismic event that strikes an urban area.

24.4.2.3 Compatible Deformation between ECC and Reinforcement

In R/ECC members with steel reinforcement, both the steel and the ECC can be considered elastic–plastic materials capable of sustaining deformation up to several percent strain. As a result, the two materials remain compatible in deformation even as both steel and ECC yield. Compatible deformation implies that no shear lag exists between the steel and the ECC, resulting in a very low level of shear stress at the steel rebar to ECC material interface. This phenomenon is unique to R/ECC members. As a result of this low interfacial stress between steel and the ECC, the bond between the ECC and reinforcement is not as critical as in normal R/C elements, as stress can be transmitted directly through the ECC material (via bridging fibers) even after microcracking. In contrast, within R/C members stress must be transferred via the rebar–concrete interface to the concrete away from the crack site. After concrete cracks in an R/C element, the concrete unloads elastically near the crack site, while the steel takes over the additional load shed by the concrete. This leads to incompatible deformation and high interface shear stress responsible for the commonly observed failure modes such as bond splitting or spalling of concrete cover. Figure 24.27a shows the stress flow in the composite, before and after matrix cracking, in R/C and R/ECC. The compatible deformation between ECC and reinforcement has been experimentally confirmed (Fischer and Li, 2002b). Figure 24.27b shows the contrasting behavior of R/ECC and R/C near the interface, revealed in a cross-sectional cut of tension-stiffening specimens. In structural elements subjected to large loads such as earthquakes, steel yielding may be expected. In R/C elements, steel yielding may be concentrated at locations where the rebar crosses the concrete cracks due to the large incompatible deformations between the steel and fractured concrete. In R/ECC elements, steel yielding can spread to a much larger volume. As a result, the distributed microcracking in ECC allows for more efficient utilization of steel reinforcement for element energy dissipation. This explains the formation of fuller hysteretic loops observed in the ECC elements discussed in Section 24.4.1 (see Figure 24.12, Figure 24.19, Figure 24.21, Figure 24.23, and Figure 24.26).

24.4.2.4 Tight Crack Width Control and Elimination of Crack Control Reinforcement

A common observation in the structural element tests described is that the cracks generated in the R/ECC have very small crack widths (see Figure 24.13, Figure 24.15, Figure 24.20, and Figure 24.24). This is because crack widths in ECC are self-controlled (Section 24.2.2). Although the presence of steel reinforcement further limits the crack width, ECC material can be easily designed to have crack widths less than 100 μm without depending on steel reinforcement. This small crack width is important with

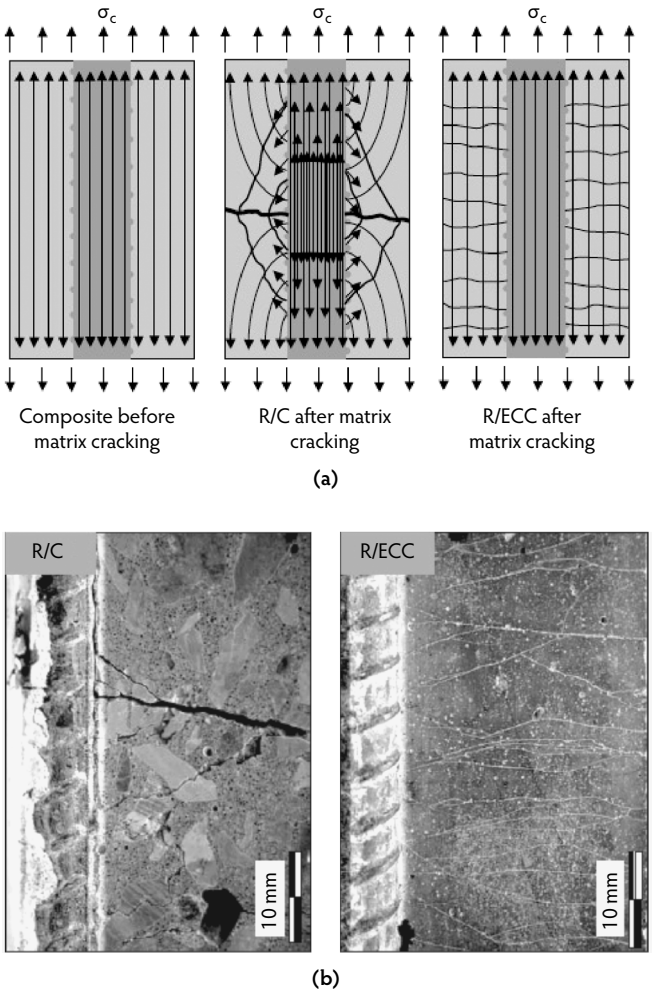

FIGURE 24.27 (a) Stress flow before and after matrix cracking. (b) On the left, brittle fracture of concrete in normal R/C causes unloading of concrete near crack, and a jump in tensile strength, straining the steel locally and resulting in high interfacial shear and bond breakage. On the right, in contrast, compatible deformation occurs between ECC and steel reinforcement with no shear lag, thus maintaining integrity of the interfacial bond. (From Fischer, G. and Li, V.C., *ACI Struct. J.*, 99(1), 104–111, 2002.)

respect to the durability of the structure (Section 24.5) and can be decisive in determining whether a structure requires repair after a major loading event (Fukuyama et al., 2007).

24.4.2.5 Transforming Material Ductility into Structural Strength

Once again, the unique feature of ECC is its ultra-high ductility. This implies that structural failure by fracture is significantly less likely in comparison to normal concrete or FRC. In traditional R/C structural design, the most common and most important material parameter of concrete is compressive strength. For this reason, structural strength (and, more generally, structural performance) is often perceived to be governed by material strength. Essentially, higher material strength (usually referred to as *compressive strength* in the concrete literature) is expected to lead to higher structural strength. This concept is valid only if the material strength property truly governs the failure mode; however, if tensile fracture failure occurs, a high-strength material does not necessarily mean higher structural strength. Instead, a high toughness material, and in the extreme, a ductile material such as ECC can lead to higher structural strength.

A number of experimental observations (Fukuyama et al., 2000; Kanda et al. 1998; Kesner and Billington, 2005; Lim and Li, 1997) provide support for the above reasoning. For example, the shear beam elements tested by Fukuyama et al. (2000) (Figure 24.18) have compressive strengths of 58.3 MPa and 52.5 MPa for concrete and ECC, respectively; however, the structural load capacity was 120 kN vs. 140 kN for the R/C and R/ECC elements, respectively (Figure 24.19). As another example, the precast in-fill wall panels (Figure 24.25) tested by Kesner and Billington (2005) for seismic retrofitting of buildings revealed that a panel with a concrete of compressive strength of 50 MPa attained a structural (shear) strength of 38 kN, while a similar panel made with ECC material of lower compressive strength (41 MPa) achieved a much higher structural strength of 56 kN (Figure 24.26). The over 35% structural strength gain in the R/ECC panel can be attributed to the material ductility of the ECC which prolonged integrity of the panel to a larger drift level. Similarly, detailed numerical analysis (Kabele, 2001) of a wall panel made with ECC demonstrated a structural strength three times that of the panel made with FRC, despite the fact that both materials had the same tensile and compressive strengths.

24.5 Durability of ECC and ECC Structural Elements

24.5.1 Material and Element Durability

As a new construction material, it is not enough to have excellent mechanical performance compared with conventional concrete or FRC. It is also important to verify the durability of the ECC material itself in various environments typical of where such materials are expected to be used. In addition, the influence of this material on structural durability performance of R/ECC must also be confirmed. In most cases, laboratory studies are performed under accelerated conditions; however, long-term performance in the field is most valuable even though it is difficult to obtain, especially for a relatively new material.

Because the greatest value of ECC lies in its superior tensile ductility, this material will likely be used in structures that impose large deformations on the material. This implies that the structure must remain serviceable even if the material undergoes tensile strain hardening accompanied by multiple microcracking. For this reason, the examination of ECC material durability should be carried out in the deformed cracked state; that is, the ECC specimen should undergo preloading to varying strain levels to deliberately create microcrack damage, prior to accelerated exposure tests. Experimental data thus determined from preloaded specimens may be considered as material durability properties under combined mechanical and environmental load. It should be noted, however, that most of these experiments were undertaken with cracked specimens in the unloaded state for experimental testing convenience. On unloading, crack widths in ECC tend to reduce by 10 to 20% from the loaded state. This reduced crack width is used in all experimental data reported. This difference from field conditions where cracks are typically under load is not expected to have a significant impact on the measured durability of ECC material or R/ECC structures but should be verified in future studies.

As will become clear in the following subsections, the durability of ECC and especially of ECC structures can be sensitive to the width of the microcracks. Microcrack widths are therefore designed to be small, typically less than 100 μm for ECC, and potentially much lower. These cracks remain small under fatigue loading, as indicated in Section 24.4.1.1; however, a recent study by Boshoff and van Zijl (2007) indicates that crack width may open wider under sustained loading due to creep mechanisms. Care must be taken for the long-term durability of a structure under combined conditions of sustained loading, deformation to the strain-hardening stage, and exposure to an aggressive environment.

In Section 24.5.2, current knowledge of ECC durability under various environments is summarized. In Section 24.5.3, the durability of R/ECC under chloride exposure is presented. This discussion is followed in Section 24.5.4 by highlights of limited long-term performance data on ECC materials already in structures exposed to the natural environment and (in one case) in combination with mechanical loads. Additional studies of ECC under various environmental or loading conditions can be found in the references in Table 24.5. Most of the durability studies covered here are for ECC reinforced with PVA fibers. The durability of PVA fiber itself has been summarized by Horikoshi et al. (2006).

TABLE 24.5 Studies of ECC Durability under Various Environments/ Loading Conditions

Environments/ Loading Conditions	Refs.
Long-term aging	Li and Lepech (2004)
Freeze–thaw cycles	Li et al. (2003)
Tropical climate exposure	Li et al. (2004)
Chloride immersion	Li et al. (2007)
Deicing salt exposure	Sahmaran and Li (2007a)
Alkali–silica reaction	Sahmaran and Li (2007b)
Fatigue	Suthiwarapirak et al. (2002)
Creep under constant load	Boshoff and van Zijl (2007)
Wheel load abrasion	Li and Lepech (2004)
Restrained drying shrinkage	Li and Stang (2005); Wang and Li (2006)
Calcium leaching	Nemecek et al. (2006)

24.5.2 ECC Durability under Various Environments

In this section, current knowledge on long-term strain capacity, as well as ECC exposed to various commonly encountered environments is summarized. These environments include freeze–thaw cycles, hot–wet cycles, chloride immersion, deicing salt exposure, and alkali–silica reaction (ASR) resistance.

24.5.2.1 Long-Term Tensile Strain Capacity

For a construction material to be considered truly durable, its mechanical properties must not degrade over time and fall below minimum design specifications. To validate ECC long-term effectiveness, a series of tensile tests were performed to determine long-term strain capacity. Due to the continued hydration process typical of cementitious materials and the delicate balance of the cement matrix, fiber, and matrix–fiber interface properties in ECC, the strain capacity of ECC evolves with age during maturing (Li and Lepech, 2004). This is exhibited in a plot of ECC strain capacity vs. age (Figure 24.28). Roughly 10 days after casting, peak strain capacity is achieved when an optimal balance of the matrix, fiber, and matrix–fiber interface properties is attained for highly saturated multiple cracking. As hydration continues, the increasing matrix toughness leads to a reduced composite ductility. Maturity of matrix and matrix–fiber properties eventually results in an ECC long-term steady strain capacity of 3%, far above

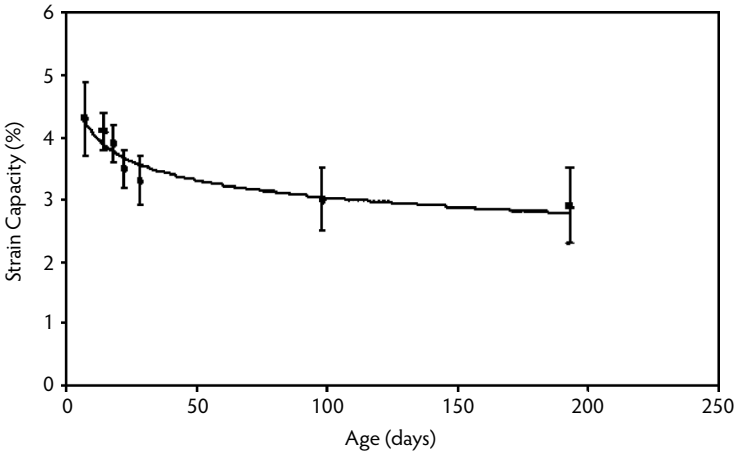

FIGURE 24.28 Tensile strain capacity of ECC as a function of age after casting. (From Li, V.C. and Lepech, M., in *Proceedings of the Transportation Research Board 83rd Annual Meeting*, Compendium of Papers CD ROM, Paper 04-4680, Transportation Research Board, Washington, D.C., 2004.)

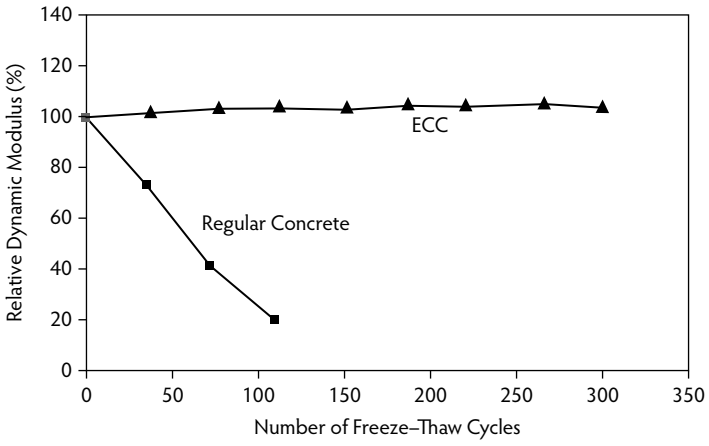

FIGURE 24.29 Relative dynamic modulus of normal concrete and three versions of ECC, all without air entrainment. (From Li, V.C. et al., *Durable Link Slabs for Jointless Bridge Decks Based on Strain-Hardening Cementitious Composites*, RC-1438, Michigan Department of Transportation, Lansing, 2003.)

the deformation demand imposed by many structural applications but significantly less than the 5% capacity seen at early age. Although long-term tests have only been carried out to 180 days, the long-term strain capacity is expected to remain at approximately 3%. The strain capacity–age curve can be seen as analogous to the compressive strength development curve in normal concrete; however, because it is not monotonically rising, the long-term value should be used for design purposes. For simplicity, 90% of the 28-day strain capacity value that approaches asymptotically to the long-term behavior may be adopted as the design strain capacity. This simplifies the design process, as the same 28-day value is used for compressive strength specification.

24.5.2.2 Freeze–Thaw Durability

Durability of non-air-entrained ECC specimens was tested by exposure to cycles of freezing and thawing, in accordance with ASTM C 666 (ASTM, 2003a). Non-air-entrained concrete specimens were also tested as reference specimens. Testing of ECC and concrete prism specimens was conducted concurrently over 14 weeks (Li et al., 2003). After 5 weeks (110 cycles), the concrete specimens had severely deteriorated, requiring removal from the freeze–thaw machine, as mandated by the testing standard; however, all ECC specimens survived the test duration of 300 cycles with no degradation of dynamic modulus (Figure 24.29). This performance resulted in a durability factor of 10 for concrete compared to 100 for ECC, as computed according to ASTM C 666. In uniaxial tension tests performed on wet-cured- and freeze–thaw-exposed ECC tensile coupons at the same age, no significant drop in strain capacity was experienced after 300 cycles. Both wet-cured and freeze–thaw specimens exhibited a strain capacity of roughly 3%.

24.5.2.3 Tropical Climate Exposure

In contrast to the freeze–thaw tests discussed above, which are designed to simulate temperature changes in winter conditions, hot-water immersion tests were conducted to simulate the long-term effects of hot and humid environments. To examine the effects of environmental exposure, hot-water immersion was performed on individual fibers, single fibers embedded in ECC matrix, and composite ECC material specimens (Li et al., 2004a). Specimens for both individual fiber pullout and composite ECC material were cured for 28 days at room temperature prior to immersion in hot water at 60°C for up to 26 weeks. After this exposure, little change was seen in fiber properties such as fiber strength, fiber elastic modulus, and elongation; however, the strain capacity of the ECC did drop from 4.5% at early age to 2.75%. Whereas the accelerated hot weather testing resulted in lower strain capacity of ECC, the 2.75% strain capacity (over 250 times that of normal concrete) seen after 26 weeks and equivalent to 70 years of natural weathering (Proctor et al., 1982) remains acceptable for most infrastructure applications.

24.5.2.4 Chloride Immersion

When ECC material is exposed to environments with high chloride concentrations, such as marine structures or for pavements and bridge decks subjected to deicing salt applications, chloride ions may alter the fiber–matrix interface and therefore the composite properties. To examine these effects, ECC coupon specimens were first preloaded under uniaxial tension to various strain levels, then exposed to a 3% NaCl solution at room temperature for 1, 2, and 3 months; they were then subsequently reloaded up to failure (Li et al., 2007). Figure 24.30 shows the data for the three sets of specimens preloaded to 0% (virgin), 0.5%, and 1.5% tensile strain. In all cases, the reloaded specimens retained multiple microcracking behavior and tensile strain capacity of more than 3%, although the average crack width increased from 40 μm to 100 μm and the tensile strength was reduced by about 10%. The wider crack width and lower tensile strength may be a result of a reduction in chemical bonding at the fiber–matrix interface, as suggested by single fiber pullout test data by Kabele at al (2007).

24.5.2.5 Deicing Salt Exposure

Sahmaran and Li (2007) studied the durability performance of non-air-entrained ECC when subjected to mechanical loading and freezing and thawing cycles in the presence of deicing salts. After 50 exposure cycles, the surface condition visual rating and total mass of the scaling residue of ECC remained within acceptable limits according to ASTM C 672 (ASTM, 2003b) (Figure 24.31a). This level of durability held true even for specimens preloaded to cracking at high deformation levels. Non-air-entrained mortar specimens were used as reference specimens. As expected, these mortar prisms under identical testing conditions deteriorated severely. Preloaded and virgin (no preloading) ECC coupon specimens were also exposed to freezing and thawing cycles in the presence of deicing salts for 25 and 50 cycles to determine their residual tensile behavior. The reloaded specimens showed negligible loss of ductility but retained multiple microcracking behavior and a tensile strain capacity of more than 3% (Figure 24.31b). It was also found that multiple microcracks due to mechanical loading healed sufficiently under freezing and thawing cycles in the presence of salt solutions and restored the specimens to nearly the original stiffness. These results confirm that ECC, both virgin and microcracked, remains durable despite exposure to freezing and thawing cycles in the presence of deicing salts.

24.5.2.6 Alkali–Silicate Reaction Resistance

Sahmaran and Li (2008a) studied the resistance of ECC to alkali–silica reaction (ASR). ECC bar specimens were immersed in alkali solution at 80°C in accordance with ASTM C 1260 (ASTM, 2007) to determine their length change due to alkali silica reaction. The ECC bar specimens containing either Class F or Class C fly ash did not show any significant expansion at the end of a 30-day soaking period (Figure 24.32). Although very fine silica sand is used in ECC, the crystalline nature of these sand particles suppresses the reactivity in an alkaline environment. Further, the presence of a high volume of fly ash decreases the pH value due to the pozzolanic reaction, making alkali–silica reaction even less likely. Finally, the presence of the PVA microfibers tends to reduce any expansion that may occur. These studies show that ECC material will not exhibit degradation due to ASR.

24.5.3 Durability of R/ECC

Increased durability of reinforced concrete is typically associated with a dense concrete matrix—that is, a very compact microstructure expected to lower permeability and reduce transport of corrosives to the steel (Beeldens and Vandewalle, 2001; Oh et al., 2002). This can be achieved with a well-graded particle size distribution, fly ash and silica fume, or low W/C ratios. These concepts, however, rely upon the concrete remaining uncracked within a structure throughout its expected service life and resisting the transport of water, chloride ions, oxygen, etc. In this presumed uncracked state, numerous concrete materials have shown promising durability in laboratory tests (Mora et al., 2003; Weiss and Shah, 2002).

In reality, however, reinforced concrete members crack due to applied structural loads, shrinkage, chemical attack, and thermal deformations, which are practically inevitable and often anticipated in

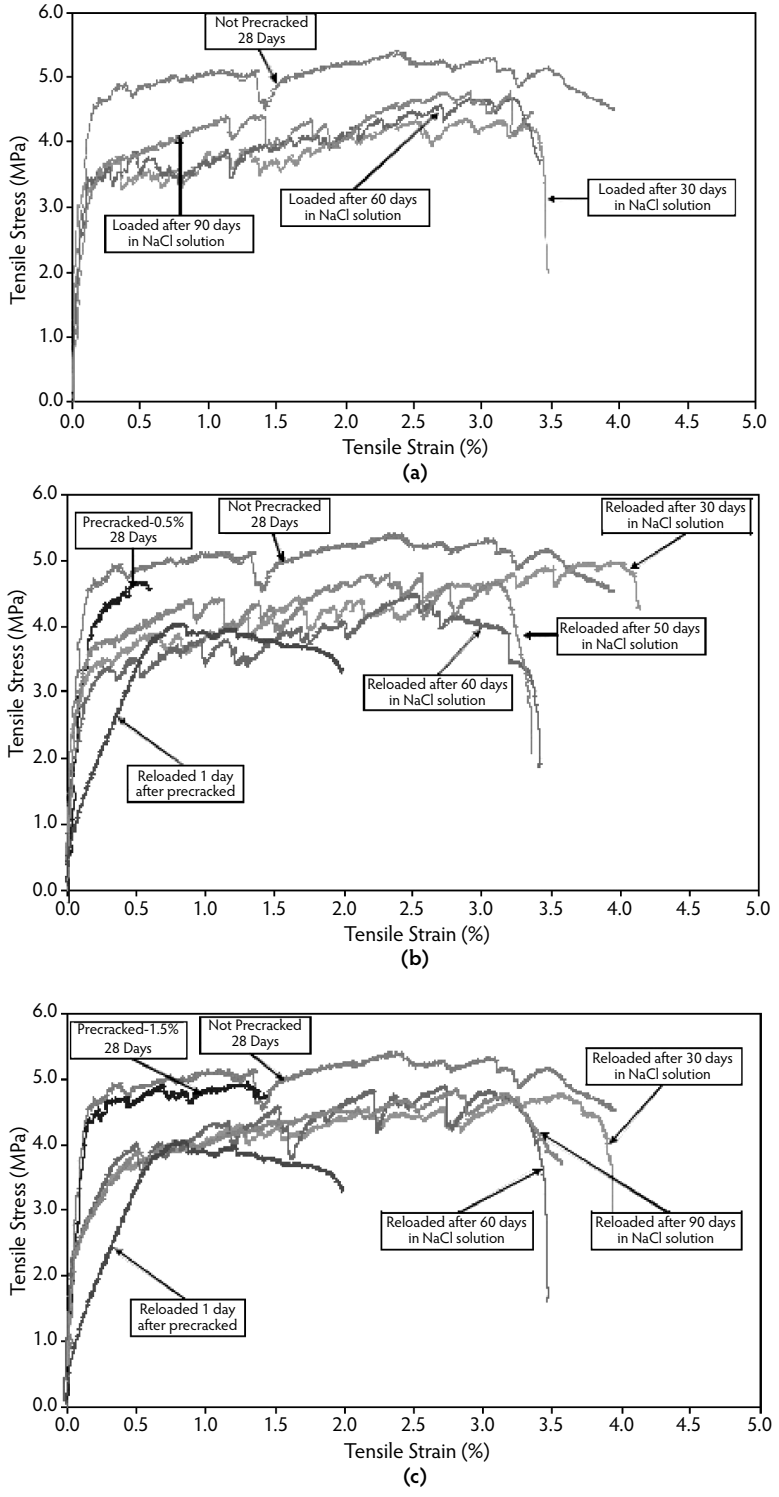

FIGURE 24.30 Tensile stress–strain curves of ECC: (a) virgin coupon specimens, (b) precracked (to 0.5%) specimens, and (c) precracked (to 1.5%) specimens, before and after being subjected to 3% NaCl solution exposure. (From Li, M. et al., in *Proceedings of the Fifth International RILEM Workshop on High-Performance Fiber-Reinforced Cement Composites (HPFRCC 5)*, Reinhardt, H.W. and Naaman, A.E., Eds., RILEM, Paris, 2007, pp. 313–322.)

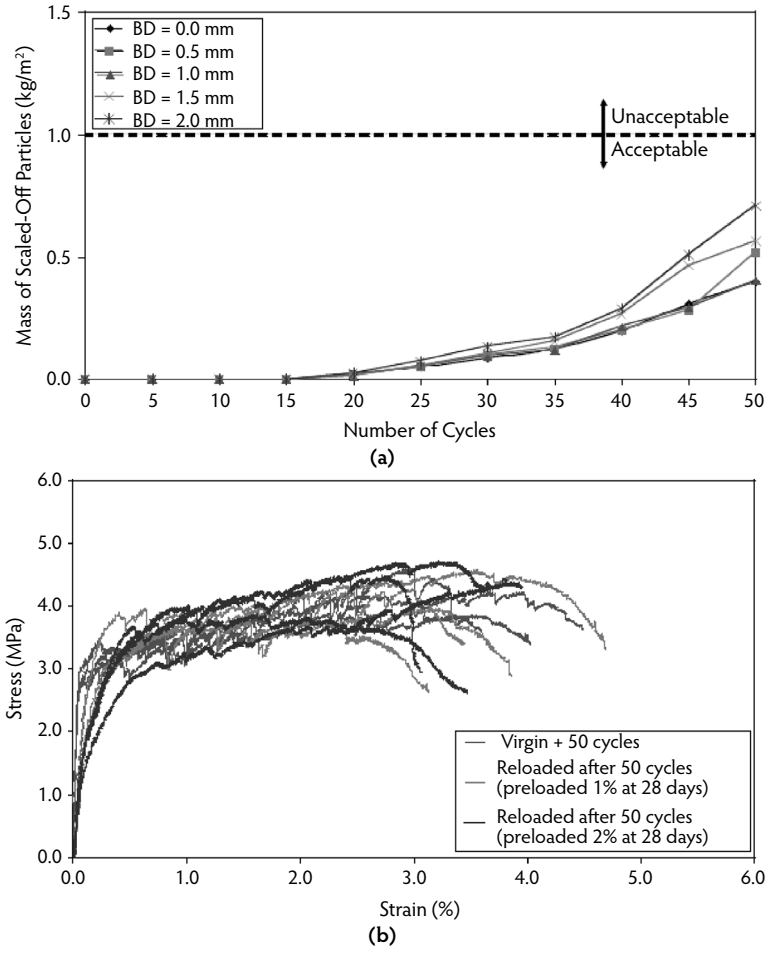

FIGURE 24.31 Effect of freeze–thaw cycles in the presence of deicing salts for (a) beams preloaded to different bending deformation (BD) levels, showing mass of scaled-off particles, and (b) coupon specimens preloaded to different levels, showing uniaxial tensile stress–strain curves after 50 cycles of exposure. (From Sahmaran, M. and Li, V.C., *J. Cement Concrete Res.*, 37, 1035–1046, 2007.)

restrained conditions (Mihashi and De Leite, 2004; Wittmann, 2002). The durability of concrete is intimately related to its transport properties—that is, the rate at which corrosives and water are able to penetrate the concrete. This is because concrete is susceptible to degradation through leaching, corrosion, sulfate attack, freezing-and-thawing damage, and other mechanisms that depend on the ingress of water. Because cracks significantly modify the transport properties of concrete, their presence greatly accelerates the deterioration process. To solve this serious problem, a fundamental solution that reduces the brittle nature of concrete is needed.

The use of ECC to replace normal concrete in steel-reinforced concrete structures has a number of implications in terms of structural durability, including:

- Alteration of transport properties in the concrete or ECC cover, thereby delaying contact of aggressive agents with steel reinforcements through the intrinsic tight crack width control of ECC
- Alteration of the nature of steel corrosion with potentials for avoiding pitting and slowing the rate of corrosion through dispersed microcracking over a region of the steel reinforcement rather than concentrating at the base of a large crack and by its resistance to cover spalling via the tensile ductility of ECC

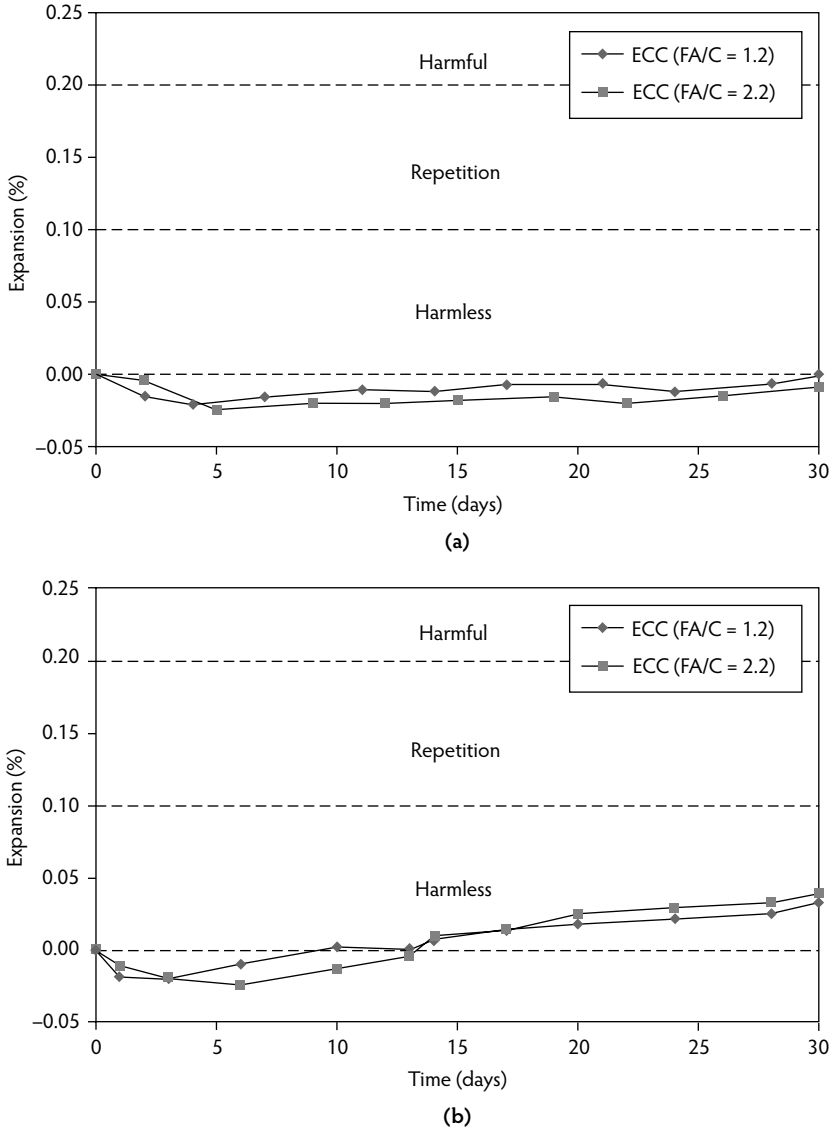

FIGURE 24.32 Length change of ECC mix with (a) Class F fly ash and (b) Class C fly ash subjected to alkali–silica reaction tests. (From Sahmaran, M. and Li, V.C., *J. Cement Concrete Composites*, 2008.)

These two alterations lead to expected improvements in structural durability due to a delay in the initiation phase of steel corrosion, and they dramatically slow the steel corrosion propagation phase. A number of experimental research efforts have been conducted that focus on the transport properties of ECC, especially when it is already in the strain-hardening stage with the presence of multiple microcracks, as well as on the behavior of steel-reinforced ECC elements in accelerated testing environments. Major findings of these two aspects are summarized in the following subsections. Recommendations for the design of R/ECC structures to protect against carbonation and chloride-ion-induced steel corrosion can be found in Rokugo et al. (2007).

24.5.3.1 Transport Properties of ECC

The most important transport properties of ECC include:

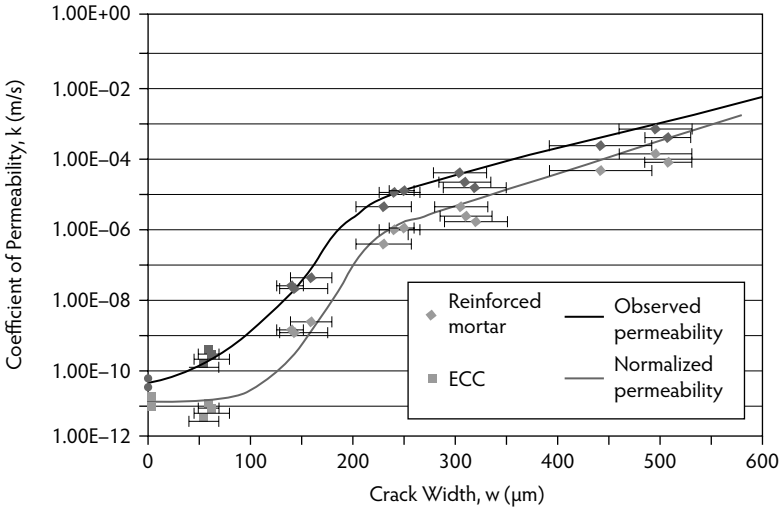

FIGURE 24.33 Permeability of precracked ECC and reinforced mortar measured as a function of crack width. (Adapted from Lepech, M.D. and Li, V.C., in *Proceedings of the 11th International Conference on Fracture (ICF XI)*, March 20–25, Torino, Italy, 2005.)

- Permeation in the presence of a hydraulic pressure, such as the condition in liquid containers and reservoir dams
- Diffusion in the presence of a ion concentration gradient, such as the condition on bridge decks, salt tanks, and marine environments
- Capillary suction induced by surface tension, of particular importance in ECC when crack width becomes very tight

All transport property tests described below were conducted at 28 days of age.

24.5.3.1.1 Water Permeation

Lepech and Li (2005a) found that cracked ECC exhibited nearly the same water permeability ($k \sim 5 \times 10^{-11}$ m/sec) as sound concrete, even when strained in tension to several percentage points (Figure 24.33). Within this study, both ECC and reinforced mortar specimens were pretensioned up to 1.5% deformation, resulting in a variety of crack widths and number of cracks among the various specimens. The permeability of these cracked materials was then determined under a hydraulic head. The dramatic rise in permeability with increasing crack width can be seen in the figure. For the ECC specimens, the crack width was intrinsically limited to about 60 μm (Section 24.2.2), regardless of the tensile deformation imposed; thus, the measured permeability was correspondingly low. Further, when normalized by number of cracks within the specimen, the comparable permeability of cracked ECC with sound material became even more apparent.

24.5.3.1.2 Chloride Diffusion

Chloride diffusion coefficients for ECC were examined by Sahmaran et al. (2007). Beam specimens were ponded in saltwater solution with 3% NaCl, according to AASHTO T259 (AASHTO, 2002). These measured values should really be regarded as the *effective chloride diffusion coefficient*, as the actual transport process is likely more complex than diffusion in a homogeneous medium without cracks. Based on tests on uncracked beams, the chloride diffusion coefficient for ECC was found to be 6.75×10^{-12} m^2/sec, compared with 10.58×10^{-12} m^2/sec based on tests on steel-reinforced mortar beams used as a control. Under high imposed bending deformation, preloaded ECC beam specimens revealed microcracks less than 50 μm and an effective diffusion coefficient significantly lower than that of similarly preloaded reinforced mortar control beams due to the tight crack widths inherent in ECC. In contrast, cracks larger than 150 μm were often produced under the same imposed deformation levels for the reinforced mortar

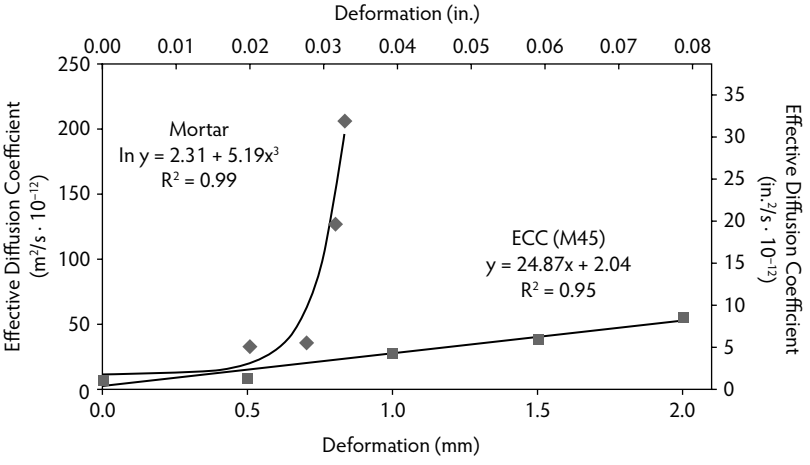

FIGURE 24.34 Diffusion coefficient vs. preloading deformation level for ECC and mortar. (From Sahmaran, M. et al., *ACI Mater. J.*, 104(6), 604–611, 2007.)

beams. Figure 24.34 shows the measured effective diffusion coefficient vs. preloading deformation level for ECC and mortar. It is revealed that the diffusion coefficient of ECC varies linearly with the number of cracks (with crack width being intrinsically constant even as beam deformation increases), whereas the diffusion coefficient of reinforced mortar is proportional to the square of the crack width. Chloride diffusion was also studied by Oh and Shin (2006) for specimens subjected up to 100,000 cycles of flexural loading. They found that the chloride diffusion coefficient did not increase significantly despite the increase number of cracks, and attribute this finding to the very fine crack width.

24.5.3.1.3 Capillary Suction

Sahmaran and Li (2008b) analyzed the water absorption and sorptivity properties of preloaded ECC, based on ASTM C 642 (ASTM, 2006) and ASTM C 1585 (ASTM, 2004) test procedures. Water absorption testing measures the mass of absorbed water per unit mass of the predried concrete material, after complete immersion in water until saturation is reached. Water absorption is expressed in terms of the volume percent of permeable pores. The sorptivity test measured the increase in mass of predried specimens at given intervals of time when permitted to absorb water by capillary suction in one direction, and it is quantified by the sorptivity index.

Figure 24.35 summarizes the findings of Sahmaran and Li which emphasized the impacts of the presence of microcracking and the water-repellent admixture on water absorption and sorptivity. From this figure, it can be seen that the presence of microcracks in ECC composites without water-repellent admixtures can lead to an exponential increase of the sorptivity index with the number of microcracks. However, sorptivity index values of cracked ECC are not particularly high when compared with those of normal concrete, probably due to the higher amount of cementitious materials, lower water/cementitious materials ratio, and high-volume fly ash content. For the ECC mixture with water-repellent admixtures, the presence of microcracks and their number had little or no effect on the sorptivity index. The water-repellent agent based on water-soluble silicon was very effective in reducing the sorptivity index of cracked ECC. ECC mixtures with water-repellent admixtures also showed lower percentages of permeable pores compared to the ECC mixtures without water-repellent admixture. In contrast to the sorptivity index, there was no significant influence of the number of cracks on the volume of permeable pores among the same ECC mixtures.

According to Neville (1995), the typical sorptivity index is 0.09 mm/min$^{1/2}$ for normal concrete with a W/C ratio of 0.4. Some other research studies suggested that ordinary Portland cement concrete with a W/C ratio of 0.4 to 0.5 would have a sorptivity index of about 0.23 mm/min$^{1/2}$ (Mehta and Monteiro, 2006). The sorptivity index for these cracked and virgin ECC specimens at a W/C ratio of 0.27 (especially

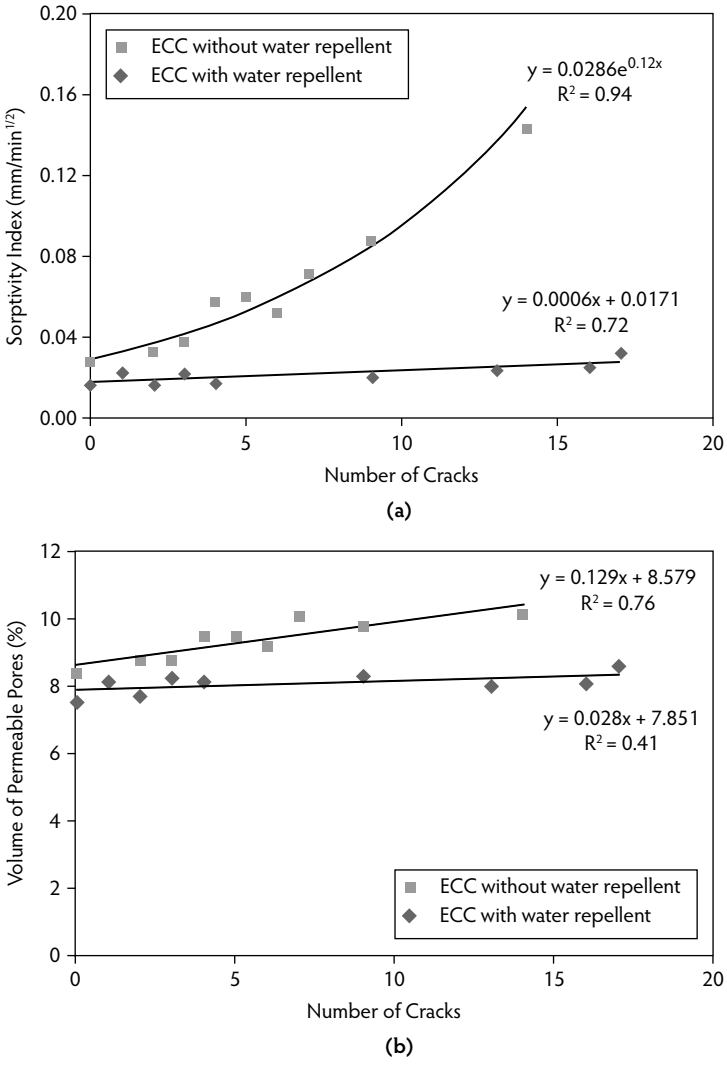

FIGURE 24.35 Capillary transport properties measured for preloaded ECC beams, showing the effects of water repellent on (a) sorptivity index and (b) volume of permeable pores as a function of the number of cracks. (From Sahmaran, M. and Li, V.C., *RILEM J. Mater. Struct*., 2008.)

for those containing water-repellent admixtures, at about 0.02 to 0.03 mm/min$^{1/2}$) was significantly lower than that for conventional concrete. Water absorption tests by Mechtcherine and Lieboldt (2007) also confirmed that ECC strained to between 0.5 and 1% showed water-retardant ability. The findings by Sahmaran and Li (2008b), together with those of Mechtcherine and Lieboldt, confirm that capillary suction does not pose a danger to the durability of ECC structures despite the expected presence of fine cracks. This risk is further reduced by the use of water-repellent admixtures. These conclusions are consistent with the findings of Martinola et al. (2004).

24.5.3.2 Corrosion Resistance in R/ECC

From the discussions presented in Section 24.5.3.1, the transport properties of ECC associated with permeation under hydraulic gradient, diffusion under ion concentration gradient, or sorption and absorption under capillary suction, all show the tendency to improve over concrete and especially cracked concrete. Given that concrete structures are designed to allow some tensile cracking and that these cracks

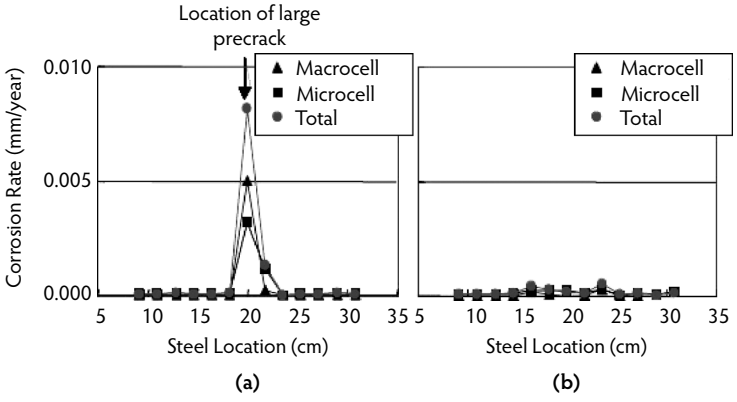

FIGURE 24.36 Measured corrosion rate along the steel rebar for preloaded (a) R/C and (b) R/ECC. (Adapted from Miyazato S. and Hiraishi, Y., in *Proceedings of the 11th International Conference on Fracture (ICFXI)*, March 20–25, Torino, Italy, 2005.)

within reinforced concrete are typically the source of corrosion due to the increased transport of water and corrosives, there is substantial potential for ECC to improve the durability of R/C structures by acting as a quality cover where all transport mechanisms are substantially inhibited. The interaction between ECC and steel reinforcement from the viewpoint of corrosion resistance has been examined. The nature and rate of steel corrosion in ECC and the spall resistance of ECC when specimens are subjected to accelerated testing conditions are presented below.

24.5.3.2.1 Nature of Steel Corrosion

A study on chloride penetration rate and corrosion rate of steel reinforcement was carried out by Miyazato and Hiraishi (2005). Preloaded R/ECC and R/C beams were exposed to a 28-day accelerated chloride environment with wet cycles (saltwater shower, 90% relative humidity, 2 days) and dry cycles (60% relative humidity, 5 days). They found that chloride penetration reached 0 to 20 mm and 80 to 100 mm in the R/ECC and the R/C beams, respectively. The total (macro- and microcell) steel rebar corrosion rate was measured to be less than 0.0004 mm/year in the R/ECC but exceeded 0.008 mm/year in the R/C beams (Figure 24.36). The observed smaller chloride penetration depth is consistent with the smaller effective diffusion coefficient found by Sahmaran et al. (2007b) discussed in Section 24.5.3.1.2. The nature of corrosion in R/ECC is decidedly different from that in R/C. Microcell currents formed between the closely spaced microcracks in the R/ECC dominate macrocell currents so a greater length of steel reinforcement experiences corrosion in the R/ECC. The much higher rebar corrosion rate concentrated at the location of the concrete crack in the R/C specimen suggests a higher tendency for pitting corrosion of the steel reinforcement to occur.

24.5.3.2.2 Corrosion Propagation and Spall Resistance

Given the tensile ductility of ECC, the ability for the cover to remain intact despite steel corrosion serves as a possibility to further prolong the service life of R/ECC structures. Sahmaran et al. (2006a) investigated R/ECC beams subjected to accelerated corrosion by electrochemical method in studies designed to induce different degrees of corrosion into the reinforcement (a single steel rebar) embedded in ECC prismatic specimens. These experiments examined the spall resistance of R/ECC cover, the influence of an intact cover on the corrosion process in the corrosion propagation phase, the rate of loss of steel by corrosion, and the residual load capacity of R/ECC elements.

The corrosion-induced crack width of mortar specimens increased with time as corrosion activity progressed. Larger crack widths, up to 2 mm wide, were obtained at higher levels of corrosion. On the other hand, crack widths of ECC remained nearly constant (~0.1 mm) with time as corrosion activity progressed, while the number of cracks on the surface of the specimen increased. The results of this study

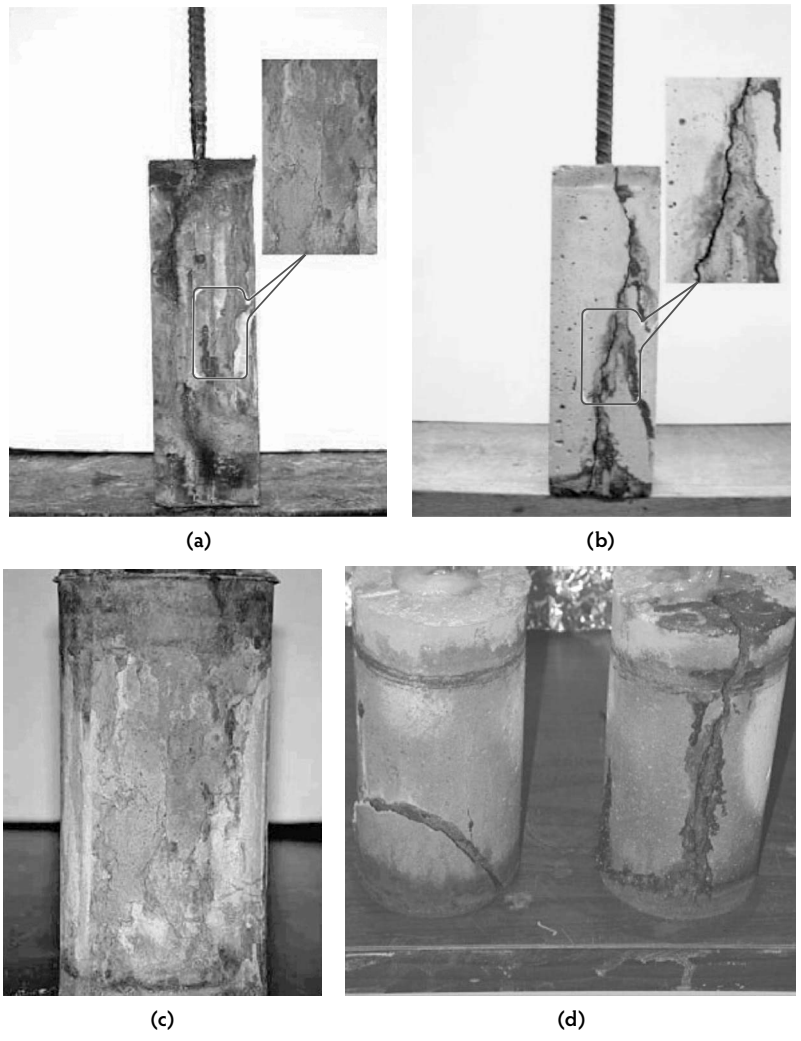

FIGURE 24.37 ECC and mortar specimens after accelerated corrosion test: (a) ECC prismatic specimen after 300 hours accelerated corrosion, (b) mortar prismatic specimen after 75 hours of accelerated corrosion, (c) ECC cylindrical specimen after 350 hours of accelerated corrosion, amd (d) mortar cylindrical specimen after 95 hours of accelerated corrosion. (From Sahmaran, M. et al., *ACI Mater. J.*, 2008.)

also showed that ECC has significant anti-spalling capability as compared to conventional mortar (Figure 24.37). If a crack width of 0.3 mm, as specified by AASHTO (2004) for the maximum crack width limit for outdoor exposures, were used to represent the serviceability limit of reinforced concrete structures, the service life of reinforced ECC would be at least 15 times that of the reinforced mortar.

Reinforcement corrosion in mortar specimens resulted in a marked reduction in stiffness and flexural load capacity. After 25 hours of accelerated corrosion exposure, the flexural strength reduced to about 34% of the original flexural capacity of the control mortar beam. In contrast, the ECC specimens after 50 hours of accelerated corrosion exposure retained almost 100% of the original flexural capacity of the control specimens. Beyond 50 hours, the flexural capacity decreased but retained over 45% that of the control specimens even after 300 hours of accelerated corrosion exposure. Longitudinal cracks due to expansion of the corrosion products also affected the failure mode of the reinforced mortar under a four-point bend load (Figure 24.38). On the other hand, ECC deterioration due to the corrosion of reinforcement did not modify the type of failure in ECC beams.

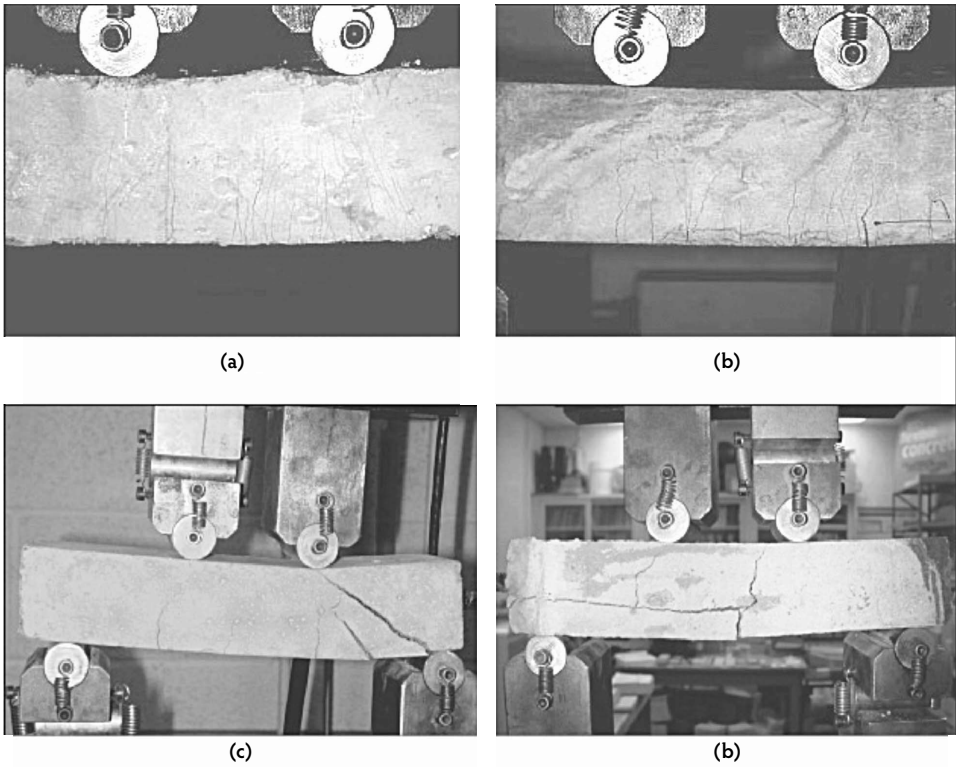

FIGURE 24.38 Types of failure of reinforced mortar and ECC beams under four-point bending test for (a) ECC before accelerated corrosion, (b) ECC after 150 hours of accelerated corrosion, (c) mortar before accelerated corrosion, and (d) mortar after 50 hours of accelerated corrosion. (Adapted from Sahmaran, M. et al., *ACI Mater. J.*, 2008.)

The loss in load-carrying capacity is related to the mass loss of the steel reinforcement due to corrosion. The percentage of steel mass losses within the ECC and mortar beams throughout the accelerated corrosion process is presented in Figure 24.39. The average percentage of mass loss of steel reinforcing bars embedded in the mortar specimens were 2.5%, 5.3%, and 11.7% at the end of 25, 50, and 75 hours of accelerated corrosion tests, respectively. On the other hand, there was nearly no mass loss of steel reinforcing bars embedded in ECC specimens after up to 50 hours of accelerated corrosion testing, and the average percentage of mass loss of reinforcing bars embedded in ECC was 17.5% at the end of 300 hours of accelerated corrosion testing. The observed superior corrosion performance of ECC compared to mortar in terms of corrosion propagation time, tight crack width, lower weight loss, and higher retention of stiffness and flexural strength is attributable to the high tensile strain capacity, strain-hardening performance, and multiple cracking behavior of ECC. Overall, the experimental results from this study suggest that the propagation period of corrosion could be safely included in estimating the service life of a structure when concrete is replaced by ECC.

24.5.4 Long-Term Performance

The long-term performance of ECC in full-scale structures has not been fully established given the relatively recent development of this material; however, at least two field demonstration studies provide limited data supporting the contention that ECC can be durable under actual field conditions. One study (Rokugo et al., 2005) involves the use of ECC for repair of a concrete gravity earth-retaining wall (18 m wide by 5 m tall) that had been damaged by alkali–silica reaction (ASR) cracking. The decision to use ECC for the 50-

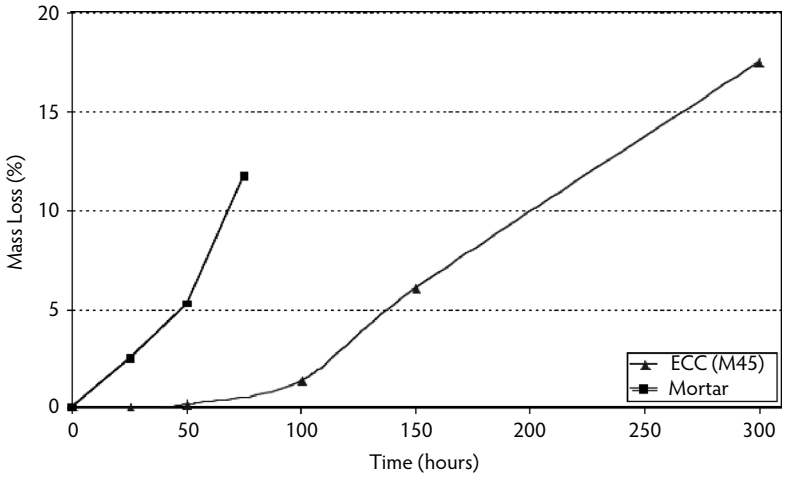

FIGURE 24.39 Mass loss vs. time for ECC and mortar corrosion specimens. (From Sahmaran, M. et al., *ACI Mater. J.*, 2008.)

to 70-mm-thick repair overlay was based on the need to prevent cracks in the substrate concrete from reflecting onto the repair layer. Such reflection was anticipated had normal concrete been used in this repair given continued ASR expansion. For demonstration, the wall was divided into nine repair blocks while a tenth block was left unrepaired. For the repaired blocks, two types of ECC—one containing 1.5% hybrid PVA and PE fibers (blocks 1 to 4) and another containing 2.1% PVA fibers (blocks 5 to 8)—were applied. In each block, welded wire mesh reinforcement, expanded metal reinforcement, or no reinforcement was used. For control, a welded wire mesh reinforced repair mortar was applied to block 9. Since 2003, when the repair took place, this wall has been continuously monitored. No cracking in the overlay was observed until 7 months after repair by ECC, while cracking was visually observed on the blocks repaired with normal mortar just 1 month after repair. The crack widths in the ECC repair blocks were less than 50 μm and 120 μm at 10 and 24 months, respectively. In contrast, the crack widths in the normal repair mortar block were 200 μm and 300 μm at 10 and 24 months, respectively. The crack patterns at 12 months and 24 months are shown in Figure 24.40. Another long-term performance verification is a small ECC patch repair placed on the bridge deck of Curtis Road over M-14 in Southern Michigan in 2002, in collaboration with the Michigan Department of Transportation (MDOT). A complete summary of this work has been outlined by Li and Lepech (2004). During this work, one section of a deteriorated bridge deck was repaired with ECC, while the remaining portion was repaired with a commercial concrete patching material commonly used by MDOT (Figure 24.41a). This repair scenario allowed for a unique comparison of ECC and concrete because both were subjected to identical environmental and traffic loads. (This road is used frequently by 11-axle trucks heavily loaded with aggregates, although it has a relatively low average daily traffic rate of 3000 vehicles/day.) The concrete repair material used was a prepackaged mixture of Portland cement and plaster of Paris. At this writing, the repaired bridge deck has experienced more than six complete Michigan winter cycles of freezing and thawing, in addition to live loads. The monitored crack width development is shown in Figure 24.41b. The ECC patch repair has survived this combined loading state with minor microcracking limited to less than 50 μm, but the concrete repair portion experienced cracking in excess of 3.5 mm and was repaired again in 2005.

24.6 Concluding Remarks

Engineered cementitious composite has a number of attractive properties. Most unique is the high tensile ductility several hundred times that of concrete with compressive strengths similar to concrete or high-strength concrete. The metal-like behavior of ECC is achieved without depending on high fiber content,

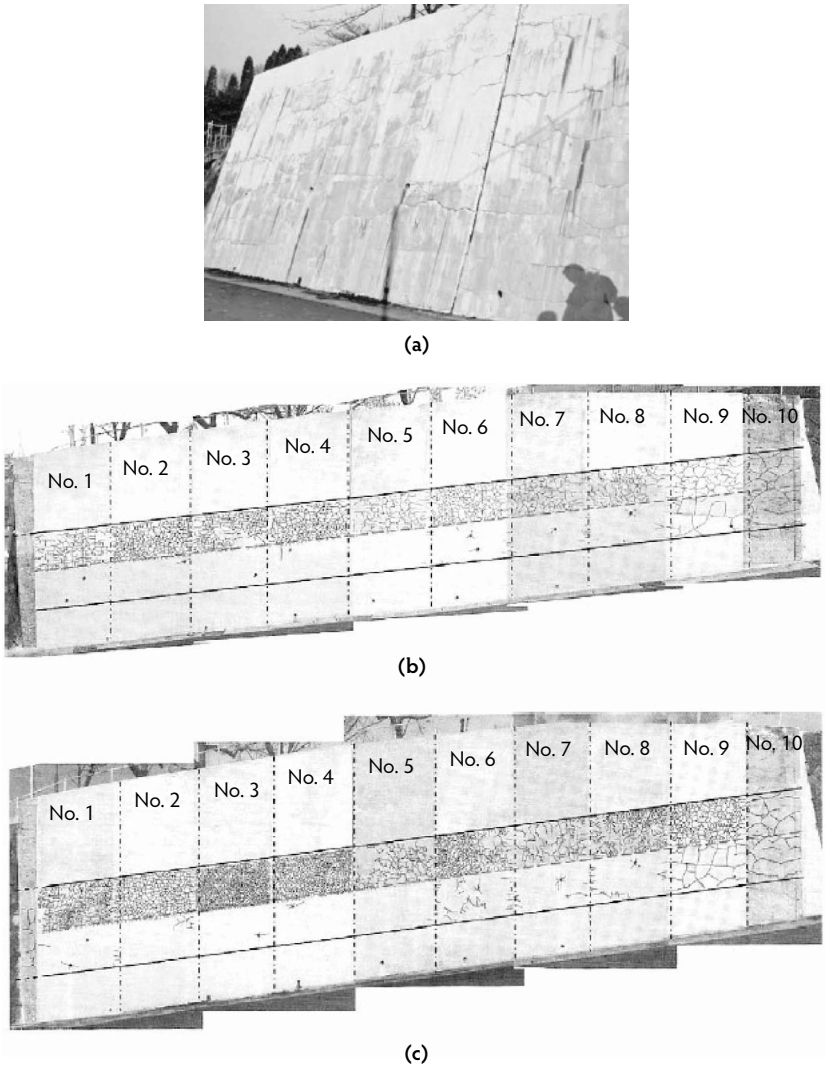

FIGURE 24.40 Cracking behavior of patched earth retaining wall: (a) Before repair, showing ASR damage; (b) after repair at 12 months; (c) after repair at 24 months. Blocks 1 to 8 used ECC, block 9 used a normal repair mortar, and block 10 was left unrepaired. (From Rokugo, K. et al., in *Proceedings of ConMat'05*, August 22–24, Vancouver, Canada, 2005.)

thus breaking the conventional wisdom of the need for a high fiber volume fraction to achieve high material performance. The moderate fiber content (2% or less by volume) makes ECC easily adaptable to construction project execution in the field or to precast plant structural element production. Indeed, ECC has demonstrated flexibility in processing routes, including on-site self-consolidating casting, and spraying, as well as off-site precasting and extrusion. Maintaining a moderately low fiber content is obviously important also for economic reasons (Li, 2004).

The large tensile ductility of ECC allows it to deform compatibly and creates a synergistic load-sharing capability with steel reinforcement in structural members. As a result, steel reinforcements in R/ECC members are better utilized in enhancing structural performance. Simultaneously, the tight crack width of ECC protects the steel reinforcement from typical corrosive processes, resulting in improved structural durability.

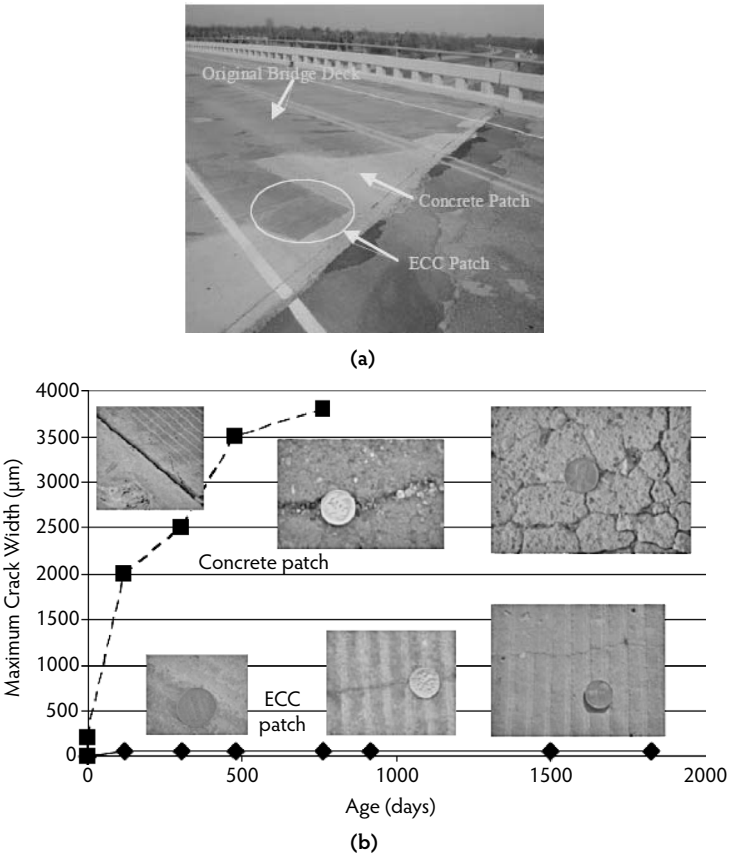

FIGURE 24.41 (a) ECC and concrete patches on the Curtis Road, Ann Arbor, MI, bridge deck; (b) maximum crack width development over time for the two materials. The concrete patch was re-repaired at about 1000 days.

In recent years, a number of full-scale applications of ECC have been carried out in various countries. Foremost among these is the use of ECC in precast R/ECC coupling beams in the core of two high-rises in Japan (Kunieda and Rokugo, 2006b; Maruta et al., 2005). This application exploits the high energy absorption capability of R/ECC to aid in the seismic resistance of these tall buildings. Other notable applications include cast-in-place ECC link slabs on bridge decks (Kim et al., 2004; Lepech and Li, 2005b) in the United States and Italy, a composite ECC/steel bridge deck in Japan (Mitamura et al., 2005), sprayed ECC tunnel linings in South Korea (Wonha, 2004), repair of the Mitaka Dam in Japan (Kojima et al., 2004), an irrigation channel repair in Japan (Kunieda and Rokugo, 2006b), and prototype pipe extrusion in Australia. Several projects in the housing and energy industries employing ECC are in various planning stages. Despite the advanced stage of development of ECC and its application readiness, a great deal of research and experimentation remain to be done. Indeed, the transformation of brittle concrete to ductile ECC offers enormous opportunities in structural innovations not possible previously.

Although safety and durability are critically important in any successful engineering project, concerns for infrastructure sustainability are growing due to greater recognition of the impact of the built environment on the natural environment. Green ECC employing industrial byproducts as components is being developed (Lepech and Li, 2008; Li et al., 2004b; Yang et al., 2007). Combined with the greater durability of ECC, such advancements offer a way to reduce environment burdens due to transportation infrastructures such as bridges and pavements (Keoleian et al., 2005; Lepech, 2006; Li et al., 2008). Sustainable infrastructures are critical to sustainable economic development in developed and developing countries. Materials technological advancements must contribute to this worldwide effort.

Acknowledgments

The author would like to acknowledge the research support of the National Science Foundation (the Biocomplexity, the Cyberinfrastructure, and the Civil, Mechanical and Manufacturing Innovation programs) and the Michigan Department of Transportation. Many former and current students, postdoctorates, and colleagues at the University of Michigan contributed to this work. Their devotion to advancing infrastructure materials is greatly appreciated. Knowledge on ECC has been greatly expanded by the intense research activities of many academic and industrial groups around the world in the last several years. Special thanks are extended to Dr. M. Lepech who reviewed a draft of this manuscript and provided helpful suggestions for improvements.

References

AASHTO. 2002. *Standard Method of Test for Resistance of Concrete to Chloride Ion Penetration*, AASHTO T 259. American Association of State Highway and Transportation Officials, Washington, D.C.

AASHTO. 2004. *LRFD Bridge Design Specifications*. American Association of State Highway and Transportation Officials, Washington, D.C.

Allen, H.G. 1971. Stiffness and strength of two glass-fiber reinforced cement laminates. *J. Composite Mater.*, 5(2), 194–207.

ASTM. 2003a. *Standard Test Method for Resistance of Concrete to Rapid Freezing and Thawing*, ASTM C 666/C 666M. American Society for Testing and Materials, Philadelphia, PA.

ASTM. 2003b. *Standard Test Method for Scaling Resistance of Concrete Surfaces Exposed to Deicing Chemicals*, ASTM C 672/C 672M. American Society for Testing and Materials, Philadelphia, PA.

ASTM. 2004. *Standard Test Method for Measurement of Rate of Absorption of Water by Hydraulic-Cement Concretes*, ASTM C 1585. American Society for Testing and Materials, Philadelphia, PA.

ASTM. 2006. *Standard Test Method for Density, Absorption, and Voids in Hardened Concrete*, ASTM C 642. American Society for Testing and Materials, Philadelphia, PA.

ASTM. 2007. *Standard Test Method for Potential Alkali Reactivity of Aggregates (Mortar-Bar Method)*, ASTM C 1260. American Society for Testing and Materials, Philadelphia, PA.

Aveston, J., Cooper, G.A., and Kelly, A. 1971. Single and multiple fracture. In *The Properties of Fiber Composites*, *Conference Proceedings*, pp. 15–24. IPC Science and Technology Press, Guildford, U.K.

Bache, H. 1981. *Densified Cement/Ultra-Fine Particle-Based Materials*, CBL Report No. 40. Aalborg Portland, Denmark.

Beeldens, A. and Vandewalle, L. 2001. Durability of high strength concrete for highway pavement restoration. In *Proceedings of Third International Conference on Concrete Under Severe Conditions (CONSEC'01)*, June 18–20, Vancouver, Canada, pp. 1230–1238.

Billington, S.L. and Yoon, J.K. 2004. Cyclic response of precast bridge columns with ductile fiber-reinforced concrete. *ASCE J. Bridge Eng.*, 9(4), 353–363.

Boshoff, W.P. and van Zijl, G.P.A.G. 2007. Tensile creep of SHCC. In *Proceedings of the Fifth International RILEM Workshop on High-Performance Fiber-Reinforced Cement Composites (HPFRCC 5)*, Reinhardt, H.W. and Naaman, A.E., Eds., pp. 87–96. RILEM, Paris.

Carpinteri, A., Gamarova, P., Ferro, G., and Plizzari, G., Eds. 2007. *Proceedings of 6th International Conference on Fracture Mechanics of Concrete and Concrete Structures (FraMCoS-6)*, June 17–22, Catania, Italy. Taylor & Francis, New York.

Chanvillard, G. and Rigaud, S. 2003. Complete characterization of tensile properties of ductal UHPFRC according to the French recommendations. In *Proceedings of the Fourth International RILEM Workshop on High-Performance Fiber-Reinforced Cement Composites (HPFRCC 4)*, Naaman, A.E. and Reinhardt, H.W., Eds., pp. 21–34. RILEM, Paris.

Curbach, M. and Jesse, F. 1999. High-performance textile-reinforced concrete. *Struct. Eng. Int.*, 9(4), 289–291.

Fischer, G. and Li, V.C. 2002a. Effect of matrix ductility on deformation behavior of steel reinforced ECC flexural members under reversed cyclic loading conditions. *ACI Struct. J.*, 99 (6), 781–790.

Fischer, G. and Li, V.C. 2002b. Influence of matrix ductility on the tension-stiffening behavior of steel reinforced engineered cementitious composites (ECC). *ACI Struct. J.*, 99(1), 104–111.

Fischer, G. and Li, V.C. 2003a. Deformation behavior of fiber-reinforced polymer reinforced engineered cementitious composite (ECC) flexural members under reversed cyclic loading conditions. *ACI Struct. J.*, 100(1), 25–35.

Fischer, G. and Li, V.C. 2003b. Intrinsic response control of moment resisting frames utilizing advanced composite materials and structural elements. *ACI Struct. J.*, 100(2), 166–176.

Fischer, G. and Li, V.C., Eds. 2006. *Proceedings, High-Performance Fiber-Reinforced Cementitious Composites (HPFRCC) in Structural Applications*. RILEM, Paris.

Fischer, G., Wang, S., and Li, V.C. 2003. Design of engineered cementitious composites for processing and workability requirements. In *Proceedings of the Seventh International Symposium on Brittle Matrix Composites*, October 13–15, Warsaw, Poland, pp. 29–36.

Fukuyama, H., Iso, M., Ogaw, A., and Suwada, H. 2007. Mitigation of damage due to crack of RC elements utilizing high-performance fiber-reinforced cementitious composites. In *Proceedings of the Fifth International RILEM Workshop on High-Performance Fiber-Reinforced Cement Composites (HPFRCC 5)*, Reinhardt, H.W. and Naaman, A.E., Eds., pp. 427–435. RILEM, Paris.

Fukuyama, H., Matsuzaki, Y., Nakano, K., and Sato, Y. 1999. Structural performance of beam elements with PVA-ECC. In *Proceedings of the Third International RILEM Workshop on High-Performance Fiber-Reinforced Cement Composites (HPFRCC 3)*, Reinhardt, H.W. and Naaman, A.E., Eds., pp. 531–542. Chapman & Hall, London.

Fukuyama, H., Matzuzaki, Y., Sato, Y., Iso, M., and Suwada, H. 2000. Structural performance of engineered cementitious composite elements. In *Proceedings of the 6th ASCCS International Conference on Steel–Concrete Composite Structures*, March 22–24, Los Angeles, CA.

Fukuyama, H., Suwada, H., and Mukai, T. 2006. Test on high-performance wall elements with HPFRCC. In *Proceedings, High-Performance Fiber-Reinforced Cementitious Composites (HPFRCC) in Structural Applications*, Fischer, G. and Li, V.C., Eds., pp. 365–374. RILEM, Paris.

Horikoshi, T., Ogawa, A., Saito, T., and Hoshiro, H. 2006. Properties of polyvinylalcohol fiber as reinforcing materials for cementitious composites. In *Proceedings, High-Performance Fiber-Reinforced Cementitious Composites (HPFRCC) in Structural Applications*, Fischer, G. and Li, V.C., Eds., pp. 145–153. RILEM, Paris.

JSCE. 2007. *Recommendations for Design and Construction of High-Performance Fiber-Reinforced Cement Composite with Multiple Fine Cracks (Draft)*, Japan Society of Civil Engineers, Tokyo [in Japanese].

Kabele, P., 2001. *Assessment of Structural Performance of Engineered Cementitious Composites by Computer Simulation*, CTU Reports No. 4, Vol. 5. Czech Technical University, Prague.

Kabele, P. and Kanakubo, T. 2007. Experimental and numerical investigation of shear behavior of PVA-ECC in structural elements. In *Proceedings of the Fifth International RILEM Workshop on High-Performance Fiber-Reinforced Cement Composites (HPFRCC 5)*, Reinhardt, H.W. and Naaman, A.E., Eds., pp. 137–146. RILEM, Paris.

Kabele, P., Novak, L., Nemecek, J., and Pekar, J. 2007. Multiscale experimental investigation of deterioration of fiber-cementitious composites in aggressive environment. In *Proc. MHM 2007: International Conference on Modelling of Heterogeneous Materials with Applications in Construction and Biomedical Engineering*, June 25–27, Prague, Jirasek, M., Bittnar, Z., and Mang, H., Eds., pp. 270–271.

Kamal, A., Kunieda, M., Ueda, N., and Nakamura, H. 2007. Assessment of crack elongation performance in RC beam repaired by UHP–SHCC. In *Proceedings of the Ninth International JSCE Summer Symposium*, September 18, Yokohama National University, Japan.

Kanakubo, T. 2006. Tensile characteristics: evaluation method for DFRCC. *J. Adv. Concrete Technol.*, 4(1), 3–17.

Kanda, T. and Li, V.C. 1999. A new micromechanics design theory for pseudo strain hardening cementitious composite. *ASCE J. Eng. Mech.*, 125(4), 373–381.

Kanda, T. and Li, V.C. 2006. Practical design criteria for saturated pseudo strain hardening behavior in ECC. *J. Adv. Concrete Technol.*, 4(1), 59–72.

Kanda, T., Watanabe, S., and Li, V.C. 1998. Application of pseudo strain hardening cementitious composites to shear resistant structural elements. In *Fracture Mechanics of Concrete Structures: Proceedings FramCoS-3*, pp. 1477–1490. AEDIFICATIO Publishers, Freiberg, Germany.

Kanda, T., Saito, T., Sakat, N., and Hiraishi, H. 2001. Basic properties of sprayed repair material based on a highly ductile FRC with PVA fiber. *Proc. Annu. Meet. JCI*, 25(1), 475–480.

Kanda, T., Kanakubo, T., Nagai, S., and Maruta, M. 2006a. Technical consideration in producing ECC pre-cast structural elements. In *Proceedings, High-Performance Fiber-Reinforced Cementitious Composites (HPFRCC) in Structural Applications*, Fischer, G. and Li, V.C., Eds., pp. 229–242. RILEM, Paris.

Kanda, T., Tomoe, S., Nagai, S., Maruta, M., Kanakubo, T., and Shimizu, K. 2006b. Full-scale processing investigation for ECC pre-cast structural elements. *J. Asian Architect. Build. Eng.*, 5(2), 333–340.

Keoleian, G.A., Kendall, A., Dettling, J.E., Smith, V.M., Chandler, R., Lepech, M.D., and Li, V.C. 2005. Life cycle modeling of concrete bridge design: comparison of engineered cementitious composite link slabs and conventional steel expansion joints. *ASCE J. Infrastructure Syst.*, 11(1), 51–60.

Kesner, K.E. and Billington, S.L. 2005. Investigation of infill panels made from engineered cementitious composites for seismic strengthening and retrofit. *ASCE J. Struct. Eng.*, 131(11), 712–720.

Kim, Y.Y., Kong, H.J., and Li, V.C. 2003. Design of engineered cementitious composite (ECC) suitable for wet-mix shotcreting. *ACI Mater. J.*, 100(6), 511–518.

Kim, Y.Y., Fischer, G., and Li, V.C. 2004. Performance of bridge deck link slabs designed with ductile ECC. *ACI Struct. J.*, 101(6), 792–801.

Kojima, S., Sakat, N., Kanda, T., and Hiraishi, T. 2004. Application of direct sprayed ECC for retrofitting dam structure surface: application for Mitaka Dam. *Concrete J.*, 42(5), 35–39 [in Japanese].

Kong, H.J., Bike, S., and Li, V.C. 2003. Development of a self-compacting engineered cementitious composite employing electrosteric dispersion/stabilization. *J. Cement Concrete Comp.*, 25(3), 301–309.

Krenchel, H. and Stang, H. 1989. Stable microcracking in cementitious materials. In *Brittle Matrix Composites 2*, Brandt, A.M. and Marshall, J.H., Eds., pp. 20–33. Elsevier, Amsterdam.

Kunieda, M. and Rokugo, K. 2006a. Measurement of crack opening behavior within ECC under bending moment. In *Proceedings, High-Performance Fiber-Reinforced Cementitious Composites (HPFRCC) in Structural Applications*, Fischer, G. and Li, V.C., Eds., pp. 313–322. RILEM, Paris.

Kunieda, M. and Rokugo, K. 2006b. Recent progress on HPFRCC in Japan: required performance and applications. *J. Adv. Concrete Technol.*, 4(1), 19–33.

Lankard, D.R. 1986. Preparation, properties and applications of cement based composites containing 5–20 percent steel fiber reinforcement. In *Steel Fiber Concrete*, Shah, S.P. and Skarendahl, A., Eds. Elsevier, Amsterdam.

Lepech, M.D. 2006. A Paradigm for Integrated Structures and Materials Design for Sustainable Transportation Infrastructure, Ph.D. thesis. University of Michigan, Ann Arbor.

Lepech, M.D. and Li, V.C. 2005a. Water permeability of cracked cementitious composites. In *Proceedings of the 11th International Conference on Fracture (ICF XI)*, March 20–25, Torino, Italy.

Lepech, M.D. and Li, V.C. 2005b. Design and field demonstration of ECC link slabs for jointless bridge decks. In *Proceedings of ConMat'05*, August 22–24, Vancouver, Canada.

Lepech, M.D. and Li, V.C. 2008. Large scale processing of engineered cementitious composites. *ACI Mater. J.*, accepted.

Lepech, M.D., Li, V.C., Robertson, R.E., and Keoleian, G.A. 2007. Design of ductile engineered cementitious composites for improved sustainability. *ACI Mater. J.*, submitted.

Leung, C.K.Y., Cheung, A.K.F., and Zhang, X. 2006. Partial use of pseudo-ductile cementitious composites in concrete components to resist concentrated stress, *Key Eng. Mater.*, 312, 319–324.

Li, M., Sahmaran, M., and Li, V.C. 2007. Effect of cracking and healing on durability of engineered cementitious composites under marine environment. In *Proceedings of the Fifth International RILEM Workshop on High-Performance Fiber-Reinforced Cement Composites (HPFRCC 5)*, Reinhardt, H.W. and Naaman, A.E., Eds., pp. 313–322. RILEM, Paris.

Li, V.C. 1993. From micromechanics to structural engineering: the design of cementitious composites for civil engineering applications. *JSCE J. Struct. Mech. Earthquake Eng.*, 10(2), 37–48.

Li, V.C. 2000. When a crack is not a crack. In *Proceedings of BMC6*, Brandt, A., Marshall, I., and Li, V.C., Eds., pp. 173-185.

Li, V.C. 2004. Strategies for high-performance fiber-reinforced cementitious composites development. In *Fiber-Reinforced Concrete: From Theory to Practice*: *Proceedings of the North American/European Workshop on Advances in Fiber-Reinforced Concrete*, Ahmad, S., di Prisco, M., Meyer, C., Plizzari, G.A., and Shah, S., Eds., pp. 93–98. Starrylink Editrice, Brescia, Italy.

Li, V.C. 2007. Integrated structures and materials design. *RILEM J. Mater. Struct.*, 40(4), 387–396.

Li, V.C. and Lepech, M. 2004. Crack-resistant concrete material for transportation construction. In *Proceedings of the Transportation Research Board 83rd Annual Meeting*, Compendium of Papers CD-ROM, Paper 04-4680. Transportation Research Board, Washington, D.C.

Li, V.C. and Leung, C.K.Y. 1992. Steady-state and multiple cracking of short random fiber composites. *ASCE J. Eng. Mech.*, 118 (11), 2246–2264.

Li, V.C., and Stang, H. 2004. Elevating FRC material ductility to infrastructure durability. In *Fiber-Reinforced Concretes (BEFIB'2004)*, di Prisco, M., Felicetti, R., and Plizzari, G.A., Eds., pp. 171–186. RILEM, Paris.

Li, V.C. and Wang, S. 2002. Failure mode and structural ductility of GFRP reinforced engineered cementitious composite beams. *ACI Mater. J.*, 99(1), 11–21.

Li, V.C. and Wang, S. 2006. Microstructure variability and macroscopic composite properties of high-performance fiber-reinforced cementitious composites. *J. Probabil. Eng. Mech.*, 21(3), 201–206.

Li, V.C. and Yang, E.H. 2007. Self-healing in concrete materials. In *Self-Healing Materials: An Alternative Approach to 20 Centuries of Materials Science*, van der Zwaag, S., Ed., pp. 161–193. Springer, New York.

Li, V.C., Wu, H.C., and Chan, Y.W. 1996. Effect of plasma treatment of polyethylene fibers on interface and cementitious composite properties. *J. Am. Ceram. Soc.*, 79(3), 700–704.

Li, V.C., Wu, C., Wang, S., Ogawa, A., and Saito, T. 2002. Interface tailoring for strain-hardening PVA-ECC. *ACI Mater. J.*, 99(5), 463–472.

Li, V.C., Fischer, G., Kim, Y.Y., Lepech, M., Qian, S., Weimann, M., and Wang, S. 2003. *Durable Link Slabs for Jointless Bridge Decks Based on Strain-Hardening Cementitious Composites*, RC-1438. Michigan Department of Transportation, Lansing.

Li, V.C., Horikoshi, T., Ogawa, A., Torigoe, S., and Saito, T. 2004a. Micromechanics-based durability study of polyvinyl alcohol-engineered cementitious composite (PVA-ECC). *ACI Mater. J.*, 101(3), 242–248.

Li, V.C., Lepech, M., Wang, S., Weimann, M., and Keoleian, G. 2004b. Development of green ECC for sustainable infrastructure systems. In *Proceedings of the International Workshop on Sustainable Development and Concrete Technology*, May 20–21, Beijing, China, Wang, K., Ed., pp. 181–192.

Li, V.C., Qian, S., Zhang, H., and Keoleian, G.A. 2008. Sustainable Infrastructure with Durable Fiber Concrete Material, paper presented at the Seventh International Congress—Concrete: Construction's Sustainable Option, July 8–10, Dundee, Scotland.

Lim, Y.M. and Li, V.C. 1997. Durable repair of aged infrastructures using trapping mechanism of engineered cementitious composites. *J. Cement Concrete Compos.*, 19(4), 373–385.

Maalej, M. and Li, V.C. 1994. Flexural/tensile strength ratio in engineered cementitious composites. *ASCE J. Mater. Civil Eng.*, 6(4), 513–528.

Maalej, M. and Li, V.C. 1995. Introduction of strain hardening engineered cementitious composites in the design of reinforced concrete flexural members for improved durability. *ACI Struct. J.*, 92(2), 167–176.

Maruta, M., Kanda T., Nagai S., and Yamamoto, Y. 2005. New high-rise RC structure using pre-cast ECC coupling beam. *Concrete J.*, 43(11), 18–26.

Martinola, G., Baeuml, M.F., and Wittmann, F.H. 2004. Modified ECC by means of internal impregnation. *J. Adv. Concrete Technol.*, 2(2), 207–212.

Mechtcherine, V. and Lieboldt, M. 2007. Effect of cracking on air-permeability and water absorption of strain hardening cement-based composites. In *Proceedings of the Fifth International RILEM Workshop on High-Performance Fiber-Reinforced Cement Composites (HPFRCC 5)*, Reinhardt, H.W. and Naaman, A.E., Eds., pp. 305–312. RILEM, Paris.

Mechtcherine, V. and Schulze, J. 2006. Testing the behavior of strain hardening cementitious composites in tension. In *Proceedings, High-Performance Fiber-Reinforced Cementitious Composites (HPFRCC) in Structural Applications*, Fischer, G. and Li, V.C., Eds., pp 37–46. RILEM, Paris.

Mehta, P.K. and Monteiro, P.J.M. 2006. *Concrete: Structure, Properties, and Materials*, 3rd ed. McGraw-Hill, New York.

Mihashi, H. and De Leite, J.P.B. 2004. State-of-the-art report on control of cracking in early age concrete. *Adv. Concrete Technol.*, 2(2), 141–154.

Mitamura, H., Sakata, N., Shakushiro, K., Suda, K., and Hiraishi, T. 2005. Application of overlay reinforcement method on steel deck utilizing engineering cementitious composites: Mihara Bridge. *Bridge Foundation Eng.*, 39(8), 88–91.

Miyazato S. and Hiraishi, Y. 2005. Transport properties and steel corrosion in ductile fiber reinforced cement composites. In *Proceedings of the 11th International Conference on Fracture (ICFXI)*, March 20–25, Torino, Italy.

Mobasher, B., Peled, A., and Pahilajani, J. 2006. Distributed cracking and stiffness degradation in fabric-cement composites. *Mater. Struct.*, 39, 317–331.

Mora, J., Aguado, A., and Gettu, R. 2003. The influence of shrinkage reducing admixtures on plastic shrinkage. *Materiales de Construccion*, 53(271–272), 71–80.

Naaman, A.E. 1992. SIFCON: tailored properties for structural performance. In *High-Performance Fiber-Reinforced Cement Composites*, Reinhardt, H.W. and Naaman, A.E., Eds., pp. 18–38. E&FN Spon, London.

Naaman, A.E. and Reinhardt, H.W. 2003. Setting the stage: toward performance-based classification of FRC composites. In *Proceedings of the Fourth International RILEM Workshop on High-Performance Fiber-Reinforced Cement Composites (HPFRCC 4)*, Naaman, A.E. and Reinhardt, H.W., Eds. RILEM, Paris.

Nemecek, J., Kabele, P., Kopecky, L., and Bittnar, Z. 2006. Leached engineered cementitious composites. In *Proceedings, High-Performance Fiber-Reinforced Cementitious Composites (HPFRCC) in Structural Applications*, Fischer, G. and Li, V.C., Eds., pp. 205–212. RILEM, Paris.

Neville, A.M. 1995. *Properties of Concrete*. 4th ed. Longman, London.

Oh, B.H. and Shin, K.J. 2006. Cracking, ductility and durability characteristics of HPFRCC with various mixture proportions and fibers. In *Proceedings, High-Performance Fiber-Reinforced Cementitious Composites (HPFRCC) in Structural Applications*, Fischer, G. and Li, V.C., Eds., pp. 213–222. RILEM, Paris.

Oh, B.H., Cha, S.W., Jang, B.S., and Jang, S.Y. 2002. Development of high-performance concrete having high resistance to chloride penetration. *Nuclear Eng. Design (Switzerland)*, 212(1–3), 221–231.

Parra-Montesinos, G. and Wight, J.K. 2000. Seismic response of exterior RC column-to-steel beam connections. *ASCE J. Struct. Eng.*, 126(10), 1113–1121.

Proctor, B.A., Oakley, D.R., and Litherland, K.L., 1982. Developments in the assessment and performance of GRC over 10 years. *Composites*, 13, 173–179.

Qian, S. 2007. Influence of Concrete Material Ductility on the Behavior of High Stress Concentration Zones, Ph.D. thesis. University of Michigan, Ann Arbor.

Qian, S. and Li, V.C. 2006. Influence of concrete material ductility on the shear response of stud connection. *ACI Mater. J.*, 103(1), 60–66.

Qian, S. and Li, V.C. 2007. Simplified inverse method for determining the tensile strain capacity of strain hardening cementitious composites. *J. Adv. Concrete Technol.*, 5(2), 235–246.

Reinhardt, H. and Naaman, A.E., Eds. 2007. *Proceedings of the Fifth International RILEM Workshop on High-Performance Fiber-Reinforced Cement Composites (HPFRCC 5)*. RILEM, Paris.

Reinhardt, H.W., Krüger, M., and Große, C.U. 2003. Concrete prestressed with textile fabric. *J. Adv. Concrete Technol.*, 1(3), 231–239.

Rokugo, K., Kunieda, M., and Lim, S.C. 2005. Patching repair with ECC on cracked concrete surface. In *Proceedings of ConMat'05*, August 22–24, Vancouver, Canada.

Rokugo, K., Kanda, T., Yokota, H., and Sakata, N. 2007. Outline of JSCE recommendation for design and construction of multiple fine cracking type fiber reinforced cementitious composite (HPFRCC). In *Proceedings of the Fifth International RILEM Workshop on High-Performance Fiber-Reinforced Cement Composites (HPFRCC 5)*, Reinhardt, H.W. and Naaman, A.E., Eds., pp. 203–212. RILEM, Paris.

Romualdi, N.P. and Batson, G.B. 1963. Mechanics of crack arrest in concrete. *Proc. ASCE Eng. Mech. J.*, 89(EM3), 147–168.

Romualdi, J.P. and Mandel, J.A. 1964. Tensile strength of concrete affected by uniformly distributed closely spaced short lengths of wire reinforcement. *Proc. ACI J.*, 61(6), 657–671.

Sahmaran, M. and Li, V.C. 2007. De-icing salt scaling resistance of mechanically loaded engineered cementitious composites. *J. Cement Concrete Res.*, 37, 1035–1046.

Sahmaran, M. and Li, V.C. 2008a. Durability of mechanically loaded engineered cementitious composites under high alkaline environment. *J. Cement Concrete Compos.*, in print.

Sahmaran, M. and Li, V.C. 2008b. Influence of microcracking on water absorption and sorptivity of ECC. *RILEM J. Mater. Struct.*, submitted.

Sahmaran, M., Li, M., and Li, V.C. 2007. Transport properties of engineered cementitious composites under chloride exposure. *ACI Mater. J.*, 104(6), 604–611.

Sahmaran, M., Li, V.C., and Andrade, C. 2008. Corrosion resistance performance of steel-reinforced engineered cementitious composites beams. *ACI Mater. J.*, in print.

Shimizu, K., Kanakubo, T., Kanda, T., and Nagai, S. 2006. In *Proceedings, High-Performance Fiber-Reinforced Cementitious Composites (HPFRCC) in Structural Applications*, Fischer, G. and Li, V.C., Eds., pp. 443–451. RILEM, Paris.

Stang, H. and Li, V.C. 1999. Extrusion of ECC-Material. In *Proceedings of the Third International RILEM Workshop on High-Performance Fiber-Reinforced Cement Composites (HPFRCC3)*, Reinhardt, H.W. and Naaman, A.E., Eds., pp. 203–212. Chapman & Hall, London.

Stang, H. and Li, V.C. 2004. Classification of fiber-reinforced cementitious materials for structural applications. In *Fiber-Reinforced Concretes (BEFIB'2004)*, di Prisco, M., Felicetti, R., and Plizzari, G.A., Eds., pp. 197–218. RILEM, Paris.

Suthiwarapirak, P., Matsumoto, T., and Kanda, T., 2002. Flexural fatigue failure characteristics of an engineered cementitious composite and polymer cement mortars. *JSCE J. Mater. Conc. Struct. Pavements*, 718(57), 121–134.

Szerszen, M.M., Szwed, A., and Li, V.C. 2006. Flexural response of reinforced beam with high ductility concrete material. In *Brittle Matrix Composites 8*, Brandt, A.M., Li, V.C., and Marshall, I.H., Eds., pp. 263–274. Woodhead, Warsaw.

Takashima, H., Miyagai, K., Hashida, T., and Li, V.C. 2003. A design approach for the mechanical properties of polypropylene discontinuous fiber reinforced cementitious composites by extrusion molding. *J. Eng. Fracture Mech.*, 70(7–8), 853–870.

Vandewalle, L. et al. 2003. RILEM TC 162-TDF: test and design methods for steel fibre reinforced concrete: sigma-epsilon-design method—final recommendation. *Mater. Struct.*, 36(262), 560–567.

Walter, R., Li, V.C., and Stang, H. 2004. Comparison of FRC and ECC in a composite bridge deck. In *Proceedings of the 5th International PhD Symposium in Civil Engineering*, June 17–19, Delft, the Netherlands, pp. 477-484.

Wang, S. 2005. Micromechanics-Based Matrix Design for Engineered Cementitious Composites, Ph.D. thesis, University of Michigan, Ann Arbor.

Wang, S. and Li, V.C. 2003. Materials design of lightweight PVA-ECC. In *Proceedings of the Fourth International RILEM Workshop on High-Performance Fiber-Reinforced Cement Composites (HPFRCC 4)*, Naaman, A.E. and Reinhardt, H.W., Eds., pp. 379–390. RILEM, Paris.

Wang, S. and Li, V.C. 2006a. High early strength engineered cementitious composites. *ACI Mater. J.*, 103(2), 97–105.

Wang, S. and Li, V.C. 2006b. Polyvinyl alcohol fiber-reinforced engineered cementitious composites: material design and performances. In *Proceedings, High-Performance Fiber-Reinforced Cementitious Composites (HPFRCC) in Structural Applications*, Fischer, G. and Li, V.C., Eds., pp. 65–73. RILEM, Paris.

Weiss, W.J. and Shah, S.P. 2002. Restrained shrinkage cracking: the role of shrinkage reducing admixtures and specimen geometry. *Mater. Struct.*, 35(246), 85–91.

Wittmann, F.H. 2002. Crack formation and fracture energy of normal and high strength concrete. *Sadhana*, 27(4), 413–423.

Wonha Co., Ltd., S. Korea. 2004. Personal communication.

Yang, E.H. and Li, V.C. 2008. Strain-hardening fiber cement optimization and component tailoring by means of a micromechanical model. *J. Construct. Build. Mater.*, in print.

Yang, E.H., Yang, Y., and Li, V.C. 2007. Use of high volumes of fly ash to improve ECC mechanical properties and material greenness. *ACI Mater. J.*, 104(6), 620–628.

Yang, Y., Lepech, M., and Li, V.C. 2005. Self-healing of engineered cementitious composites under cyclic wetting and drying. In *Proceedings of the International Workshop on the Durability of Reinforced Concrete Under Combined Mechanical and Climatic Loads (CMCL)*, October 27–28, Qingdao, China, pp. 231–242.

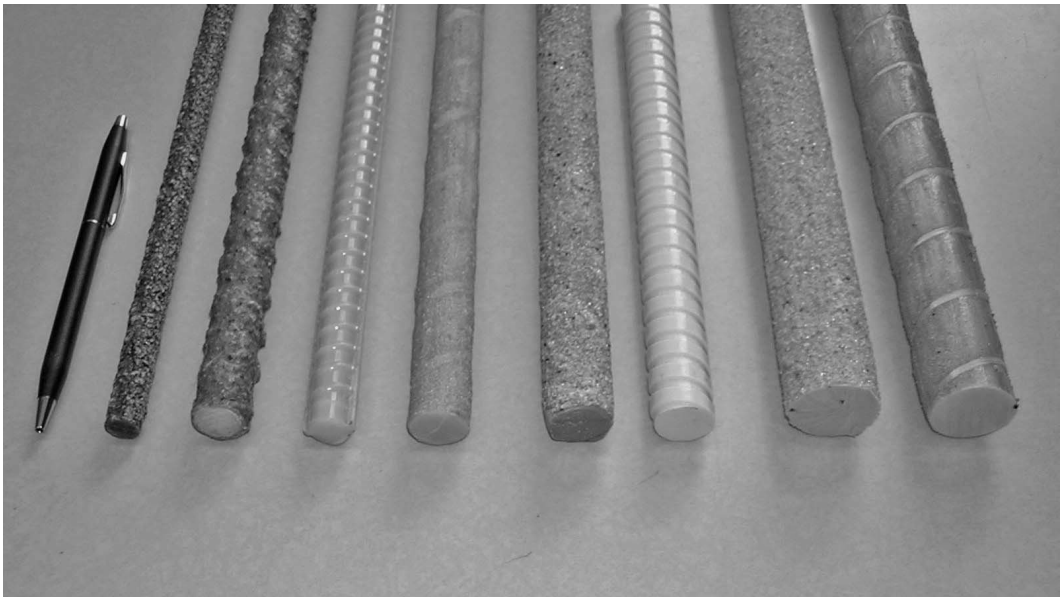

Typical FRP reinforcing bars for concrete members.